https://doi.org/10.5194/angeo-2023-27
Preprint. Discussion started: 16 August 2023


Annales Geophysicae Discussions
Open Access

# A statistical study of the magnetic signatures of the unique Tonga volcanic explosion of 15 January 2022

Leonid F. Chernogor

[1]Department of Space Radio Physics V. N. Karazin Kharkiv National University, Kharkiv, 61022 Ukraine

*Correspondence to*: Leonid F. Chernogor (Leonid.F.Chernogor@gmail.com)

**Abstract.** For the first time, a statistical study has been conducted of the geomagnetic bay and quasi-periodic disturbances based on the datasets collected at 19 recording stations participating in INTERMAGNET Magnetic Observatories. In order to identify the disturbances from the volcanic explosion, a preliminary analysis has been used of the state of space weather during the catastrophic Tonga volcanic explosion of 15 January 2022. We summarize the main results as follows: The non-monotony of the variations in the strength of all geomagnetic field components increased appreciably on the day of the explosion as compared to the variations observed during the days used as a quiet time reference, while the eastward component of the geomagnetic field exhibited an up to 60-nT increase in variability. The duration and time delay of the bay disturbances increased with distance from the volcano, while their amplitude decreased. The propagation speeds of the bay disturbances at various observatories were determined to be in the 700–1,000 m/s range. Six groups of time delays of quasi-sinusoidal disturbances have been identified in a simultaneous analysis for the first time; they correspond to the apparent speeds of 4 km/s, 1.5 km/s, 1 km/s, as well as 500 m/s, 313 m/s, and 200 m/s. The time delay in each group increased with distance away from the volcano. The agreement between theoretical estimates and the observational data testify to the adequacy of the mechanism adopted for the generation of the disturbances.

## 1 Introduction

Five underwater Tonga volcanic explosions (20°54′ S, 175°38′ W) were observed to occur over the 04:00–05:00 UTC period on 15 January 2022, with the second explosion at 04:15 UTC being the most powerful (Adushkin et al., 2022; Astafyeva et al., 2022; Matoza et al., 2022a; Matoza et al., 2022b). The gas emissions reached 50–58-km altitude producing the highest recorded eruption column, whereas the eruption columns of Krakatoa volcano on 26–27 August 1883 reached only 40–55 km (Chernogor, 2012; McNutt et al., 2015). The Tonga volcanic eruption thermal energy is estimated to be ~$3.9 \cdot 10^{18}$ J, and the mean thermal power to be $9.1 \times 10^{12}$ W (Chernogor, 2022a; Chernogor, 2022e; Chernogor, 2023a). The mass of the erupted material attained 2.9 Gt and their volume $1.9 \times 10^{9}$ m$^3$. The volcanic explosivity index (VEI) did not exceed 5.8, and the explosive energy was estimated to be in the range from 4–18 Mt of TNT to 478 ± 191 Mt of TNT (Adushkin et al., 2022; Astafyeva et al., 2022; Kulichkov et al., 2022).

https://doi.org/10.5194/angeo-2023-27
Preprint. Discussion started: 16 August 2023




The Tonga volcanic explosion was accompanied by essential disturbances in all components of the Earth (lithosphere, ocean)–atmosphere–ionosphere–magnetosphere system (Chernogor, 2022a; Chernogor, 2022b; Chernogor, 2022c; Chernogor, 2022d; Chernogor, 2022e; Chernogor, 2023a; Chernogor, 2023b). More than 50 studies were concerned with the effects caused by the volcanic explosion. Measurements were made of the earthquake of Richter magnitude 5.8 (Poli and Shapiro, 2022), of seismic wave propagation (Diaz et al., 2022; Matoza et al., 2022a; Matoza et al., 2022b; Poli and Shapiro, 2022), of tsunamis (Carvajal et al., 2022; Imamura et al., 2022; Kubota et al., 2022; Ramírez-Herrera et al., 2022; Tanioka et al., 2022; Terry et al., 2022), of Lamb waves (Kubota et al., 2022; Kulichkov et al., 2022; Lin et al., 2022; Matoza et al., 2022a; Matoza et al., 2022b; Otsuka et al., 2022), of atmospheric gravity, infrasound, and sound waves (Burt et al., 2022; Chen et al., 2022; Chernogor and Shevelev, 2022; Lin et al., 2022; Matoza et al., 2022a; Matoza et al., 2022b; Wright et al., 2022), as well as observations were made of volcanic signatures in the atmosphere and ionosphere (Aa et al., 2022a; Aa et al., 2022b; Ajith et al., 2022; Astafyeva et al., 2022; Chen et al., 2022; Chernogor et al., 2022; Harding et al., 2022; Hong et al., 2022; Lin et al., 2022; Muafiry et al., 2022; Rakesh et al., 2022; Shinbori et al., 2022; Sun et al., 2022a; Sun et al., 2022b; Themens et al., 2022; Zhang et al., 2022a; Zhang et al., 2022b).

Theoretical studies of the chain of physical processes were performed by (Chernogor, 2012; Chernogor, 2022a; Chernogor, 2022b; Chernogor, 2022c; Chernogor, 2022d; Chernogor, 2022e; Chernogor, 2023a; Chernogor, 2023b).

Sun et al. (2022b) have estimated disturbances in the electric current in the ionospheric $E$ region caused by the Tonga volcanic explosion by making use of the data on geomagnetic field variations acquired by the global network of magnetometers. The $E$-region current density was estimated to be $J \approx$ 22–55 mA/m, which changed the eastward components, $Y$, of the geomagnetic field by ~20–50 nT. The leading front of the disturbance traveled with a propagation speed of 740 m/s. Le et al. (2022) investigated the effect that the volcano had on the equatorial electrojet and revealed the reversal of the electrojet direction due to a strong eastward zonal wind.

The explosion was also accompanied by variations in the geomagnetic field (Adushkin et al., 2022; Chernogor, 2023c; Chernogor and Holub, 2023a, 2023b; Iyemori et al., 2022; Le et al., 2022; Schnepf et al., 2022; Soares et al., 2022; Yamazaki et al., 2022). Adushkin et al. (2022) have described waves and disturbances in the atmospheric electric and magnetic fields. The data collected at 14 stations in the global network of observatories, INTERMAGNET, which are located in the 2.790–6.225 Mm distance range from the volcano, have been used for investigating the magnetic effect. The disturbances in the geomagnetic field have been deduced to occur on a global scale, and two groups of disturbance have been revealed. In the first group, the disturbances were virtually synchronously observed immediately after the explosion, whereas in the second group, the magnetic disturbances appeared after the arrival of Lamb waves. Soares et al. (2022) described quasi-periodic disturbances in the magnitude of the eastward component, $Y$, with amplitude of ~3 nT and an ~4-min period observed with onset time delay of 10 min at 835-km distance from the volcano. The geomagnetic variations at 3.8-mHz (period of $T \approx 4.4$ min) have been analyzed by (Iyemori et al., 2022; Yamazaki et al., 2022), who relate these variations to the acoustic resonance. It is important to note that the oscillations at 3.8 mHz were observed simultaneously both in the vicinity of the volcano (API station) and in the magnetically conjugate region (HON station). The amplitudes of these

https://doi.org/10.5194/angeo-2023-27
Preprint. Discussion started: 16 August 2023




virtually synchronous oscillations were observed to be 2 nT and 0.2 nT, respectively, while the time delay of the magnetic effect did not exceed 6 min. However, analogous oscillations were not observed at distances, *r*, greater than 2.7 Mm. The study by Schnepf et al. (2022) is concerned with the investigation of geomagnetic variations in the 3–8-min period range with amplitude of ~1 nT that were observed with a time delay of ~30 min (propagation speed of ~470 m/s). The authors relate these variations to the ionospheric wave, which was generated by the volcano, and explain the variations in the 13–93- and 5–100-min period ranges by the effects of tsunami and of atmospheric and ionospheric sources. Harding et al. (2022) describe the multi-instrument studies of the magnetic effect of Tonga volcano. They utilized the data collected by magnetometers at the ground and onboard the ICON and Swarm spacecraft to study the effect that the volcanic explosion had on neutral winds and the ionospheric dynamo current system on a global scale. Despite significant progress made in understanding the geomagnetic field disturbances related to the Tonga volcanic explosion, a further statistical and spectral analyses of these variations is to advance understanding of this scientific issue.

The purpose of this paper is to present, for the first time, the inferences of the statistical and spectral analyses of the bay and quasi-periodic disturbances in the geomagnetic field that were observed to occur after the Tonga volcanic explosion on 15 January 2022. The data used for this research have been acquired at nineteen INTERMAGNET observatories closest to the volcano.

## 1 Information on Tonga volcano

Tonga volcano is located ~200 m below the oceanic surface. An intense volcanic eruption was recorded to occur from ~04:00 UTC to ~16:00 UTC on 15 January 2022 when the rates of eruption attained 67 kt/s or 44,000 m$^3$/s. In total, the volcano was active for over 12 ± 1 h, whereas the energy of the blast wave was estimated to be 16–18 Mt TNT [Chernogor, 2022a; Chernogor, 2022e; Chernogor, 2023a]. Generally, Tonga volcano is among the five most powerful on record (Table 1).

Table 1. Basic information on volcanos.

| Information | Krakatoa | St. Helen | El Chichón | Pinatubo | Tonga |
|---|---|---|---|---|---|
| Date | 26–27 August 1883 | 18 May 1980 | 29 March and 3–4 April 1982 | 15 June 1991 | 15 January 2022 |
| Country, location | Indonesia | USA, Skamania County | Mexico | Philippines | Kingdom of Tonga |
| Geographic coordinates | 6°06′ N, 105°25′ E | 46°12′ N, 122°11′ W | 17°22′ N, 93°14′ W | 15°7.8′ N, 120°21′ E | 20°54′ S, 175°38′ W |
| Total eruptive mass (kg) | $2.9 \times 10^{13}$ | $1.3 \times 10^{12}$ | $1.3 \times 10^{12}$ | $1.3 \times 10^{13}$ | $2.9 \times 10^{12}$ |

https://doi.org/10.5194/angeo-2023-27
Preprint. Discussion started: 16 August 2023



| | | | | | |
|---|---|---|---|---|---|
| Eruption column height (km) | 40–55 | 19–25 | 30–32 | 33 | 50–58 |
| Mean mass flow rate (kg/s) | $5.5 \times 10^8$ | $2 \times 10^7$ | $1.5 \times 10^8$ | $8 \times 10^8$ | $6.7 \times 10^7$ |
| VEI | 6 | 5 | 5 | 6 | 5–6 |
| Magnitude | 6.5 | 5.1 | 5.1 | 6.1 | 5.5 |
| Intensity | 11.7 | 10.3 | 11.2 | 12 | 10.8 |
| Notes | Current altitude 813 m, Vent 120 m | Altitude 2,549 m, Reduced by 400 m | Altitude 1,150 m, Vent 1,000 m, Crater depth 300 m | Altitude 1,486 m; before 1991, 1,745 m | Plinian underwater eruption at a 200 m depth |

The volcanic magnitude can be estimated using the following formula of McNutt et al. (2015):

$$M = \log m - 7$$

where $m$ is the erupted mass (in kg). Substituting $m = 2.9 \times 10^{12}$ kg yields $M \approx 5.5$, whereas the most powerful Krakatoa volcanic has a magnitude of $M \approx 6.5$ (Table 1). The mass eruption rate, $\dot{m}$, is characterized by the intensity, given by the relation (McNutt et al., 2015):

$$I = \log \dot{m} + 3.$$

Here $\dot{m}$ is in kg/s. Given the averaged value of the mass eruption rate $\dot{m} \approx 6.7 \times 10^7$ kg/s, the intensity is $I \approx 10.8$, whereas $I \approx 11.7$ for Krakatoa volcano (Table 1).

## 3 Analysis of the state of space weather

The state of space weather over the 12–18 January 2022 period is characterized by the data retrieved from the World Data Center for Geomagnetism, Kyoto https://wdc.kugi.kyoto-u.ac.jp/ and from the Goddard Space Flight Center Space Physics Data Facility https://omniweb.gsfc.nasa.gov/form/dx1.html. The sunspot number did not exceed ~100, while the daily 10.7 cm solar radio flux ($F_{10.7}$) was in the ~100–120 sfu range (1 sfu = $10^{-22}$ W /(Hz m$^2$)). A substantial increase (by a factor of a few times) in the solar wind parameters took place during the 14/15 January 2022 UTC night. The interplanetary magnetic field $B_z$ component showed a decrease from ±4 nT to –14 nT, the equatorial $D_{st}$ index exhibited a decrease from 10 nT to –90 nT, while the auroral activity index $A_p$ showed an increase from ~5 nT to 67 nT, and the 3-h range planetary $K_p$ index from ~1 to 5.7. Thus, a *G2*-moderate *geomagnetic storm took place over the* 14/15 January 2022 night. The recovery phase of the storm proceeded over the 15–18 January 2022 period. It should be noted that the auroral electrojet (AE) index was observed to be ~100 nT over 04:00–11:00 UTC period on 15 January 2022, i.e., geomagnetic conditions were quiet, whereas before

https://doi.org/10.5194/angeo-2023-27
Preprint. Discussion started: 16 August 2023


04:00 UTC and after ~11:00–12:00 UTC, the AE index exceeded 500 nT, which indicated a geomagnetic disturbance (substorm). 13 January 2022, when the geomagnetic conditions were quietest, was chosen to be a quiet time reference. 17 January 2022 is also used, although partially, as a quiet time reference.

## 4 Instrumentation and techniques

The study is based on data from the INTERMAGNET magnetic observatory network, which were accessed through the https://www.intermagnet.org/. The list of the stations is presented in Table 2, and their locations around Tonga volcano are depicted in Figure 1. It is important to note that the stations are located around all cardinal points as seen from the volcano. We have analyzed the temporal variations in the northward, $X$, eastward, $Y$, and vertical, $Z$, components of the geomagnetic field acquired on 12, 13, 15, 16, 17, and 18 January 2022 with 1-min temporal resolution and the root-mean-square error not exceeding 1 nT.

The algorithm for finding the geomagnetic field response to Tonga volcanic explosion is as follows:

(1) Since the variations in the geomagnetic field may be caused by many powerful sources releasing significant amounts of energy, any characteristic changes in the variations in the strength of the $X$, $Y$, and $Z$ components that were observed to occur after the volcanic explosion and could be associated with the explosion are highlighted at the first stage of employing the algorithm. This condition is necessary but insufficient.

(2) At the second stage, the variations analogous to those that occurred on quiet time days and were due to, for example, diurnal variation, the solar terminator, etc., are filtered out.

(3) Next, the possible time delays and apparent speeds are determined. The time delay should increase with distance from the volcano.

(4) If some apparent speeds at different stations are substantially close to each other, they are included in a particular statistic. The closeness of the apparent speeds in this particular statistic is considered a sufficient condition for this particular disturbance to be due to the volcanic explosion.

(5) The physical significance of the apparent speeds is an additional sufficient condition: these speeds must correspond to the known speeds of waves of particular physical nature.

(6) The results obtained are compared, if possible, with the results obtained for the volcanoes that exploded before.

It should be emphasized that the variations in the geomagnetic field components were generally more or less smooth on the days used as a quiet time reference, whereas they became non-monotonical after the Tonga volcanic explosion when aperiodic and quasi-periodic variations were observed to occur in the magnitude of the geomagnetic field components. The moving average process was first created by averaging, over 60-min intervals, the raw data $X(t)$, $Y(t)$, and $Z(t)$ sampled at a 1-min time step to be subtracted from the temporal variations in the raw data to yield the $\Delta X(t)$-, $\Delta Y(t)$-, and $\Delta Z(t)$-component deviations, which were finally subjected to the Fourier and wavelet transforms (Chernogor, 2008).

https://doi.org/10.5194/angeo-2023-27
Preprint. Discussion started: 16 August 2023


Annales Geophysicae Discussions
Open Access
EGU

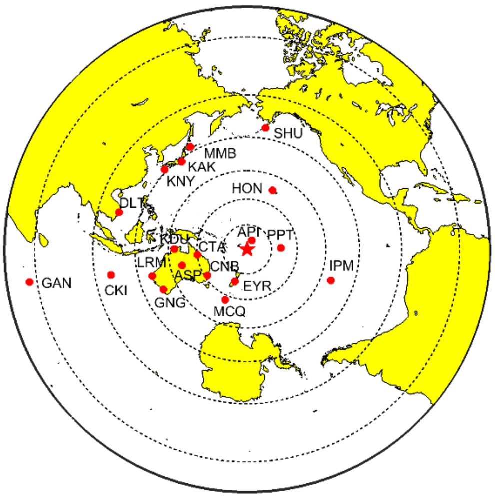


**Figure 1: Map showing the sites of the recording stations. Star designates the volcano.**

Table 2. Information on the INTERMAGNET magnetic observatories.

| IAGA[a] station code | Geographic latitude and longitude | Magnetic latitude and longitude | Country | Distance from the explosion (km) |
|---|---|---|---|---|
| Apia (API) | 13.8155° S<br>171.7812° W | 15.01° S<br>96.77° W | Western Samoa | 840 |
| Pamatai (Papeete) (PPT) | 17.5670° S<br>149.5740° W | 15.15° S<br>74.29° W | French Polynesia | 2,730 |
| Eyrewell (EYR) | 43.4740° S<br>172.3930° E | 46.56° S<br>106.28° W | New Zealand | 2,790 |
| Canberra (CNB) | 35.3200° S<br>149.3600° E | 41.75° S<br>132.81° W | Australia | 3,806 |
| Charters Towers (CTA) | 20.0900° S<br>146.2640° E | 27.05° S<br>138.47° W | Australia | 3,990 |
| Macquarie Island | 54.5000° S | 59.32° S | Australia | 4,349 |

https://doi.org/10.5194/angeo-2023-27
Preprint. Discussion started: 16 August 2023

Annales Geophysicae Discussions

| | | | | |
|---|---|---|---|---|
| (MCQ) | 158.9500° E | 116.38° W | | |
| Honolulu (HON) | 21.3200° N<br>158.0000° W | 21.65° N<br>88.98° W | United States of America | 5,024 |
| Alice Springs (ASP) | 23.7620° S<br>133.8830° E | 31.83° S<br>151.19° W | Australia | 5,210 |
| Kakadu (KDU) | 12.6900° S<br>132.4700° E | 20.96° S<br>153.66° W | Australia | 5,602 |
| Isla de Pascua Mataveri (IPM) | 27.1713° S<br>109.4200° W | 19.48° S<br>34.44° W | Chili | 6,675 |
| Gingin (GNG) | 31.3560° S<br>115.7150° E | 40.34° S<br>170.60° W | Australia | 6,887 |
| Learmonth (LRM) | 22.2200° S<br>114.1000° E | 31.28° S<br>172.67° W | Australia | 7,233 |
| Kakioka (KAK) | 36.2320° N<br>140.1860° E | 28.13° N<br>150.18° W | Japan | 7,852 |
| Kanoya (KNY) | 31.4200° N<br>130.8800° E | 22.70° N<br>158.28° W | Japan | 8,135 |
| Memambetsu (MMB) | 43.9100° N<br>144.1900° E | 36.09° N<br>147.57° W | Japan | 8,265 |
| Shumagin (SHU) | 55.3500° N<br>160.4600° W | 54.46° N<br>100.96° W | United States of America | 8,557 |
| Dalat (DLT) | 11.9400° N<br>108.4800° E | 2.60° N<br>178.89° W | Vietnam | 9,068 |
| Cocos (Keeling) Islands (CKI) | 12.1875° S<br>96.8336° E | 21.21° S<br>168.97° E | Australia | 9,308 |
| Gan International Airport (GAN) | 0.6946° S<br>73.1537° E | 8.34° S<br>145.40° E | Maldives | 12,210 |

[a]IAGA stands for International Association of Geomagnetism and Aeronomy

https://doi.org/10.5194/angeo-2023-27
Preprint. Discussion started: 16 August 2023


## 5 Analysis of temporal variations in geomagnetic field strengths

A preliminary analysis of the temporal dependences $X(t)$, $Y(t)$, $Z(t)$ and of their time derivatives $\dot{X}(t)$, $\dot{Y}(t)$, $\dot{Z}(t)$ determined that the character of the variations on 15 January 2022 was markedly different from that observed during the quiet time reference periods when the variations were smoother and the values of the derivatives were noticeably smaller.

*API Station.* Geomagnetic bay disturbances were absent on 13 January 2022 (Figure 2), and the magnitude of fluctuations did not exceed 1 nT. On 17 January 2022, used as a quiet time reference, synchronous geomagnetic bay disturbances were absent (Figure 2). The magnitudes of fluctuations in all components exhibited insignificant variability within the ±1-nT limits.

On 15 January 2022, the geomagnetic bay disturbances appeared with a time delay, $\tau$, of ~16 min and lasted for $\Delta T_X \approx 120$ min, $\Delta T_Y \approx 146$ min, and $\Delta T_Z \approx 130$ min. They were observed to occur virtually synchronously in all three components of the geomagnetic field (Figure 2). The peak deviations from the trend in the bay disturbances are estimated to be $\Delta X \approx 16$ nT, $\Delta Y \approx 26$ nT, and $\Delta Z \approx -13$ nT. The more rapid fluctuations are superimposed upon these slow enough variations; they appear with time delays of $\Delta t_0 \approx 6$ min, $\Delta t_1 \approx 8.5$ min, $\Delta t_2 \approx 14$ min, $\Delta t_3 \approx 19$ min, $\Delta t_4 \approx 33$ min, $\Delta t_5 \approx 50$ min, and $\Delta t_6 \approx 75$ min (Table 3).

https://doi.org/10.5194/angeo-2023-27
Preprint. Discussion started: 16 August 2023

Annales Geophysicae Discussions

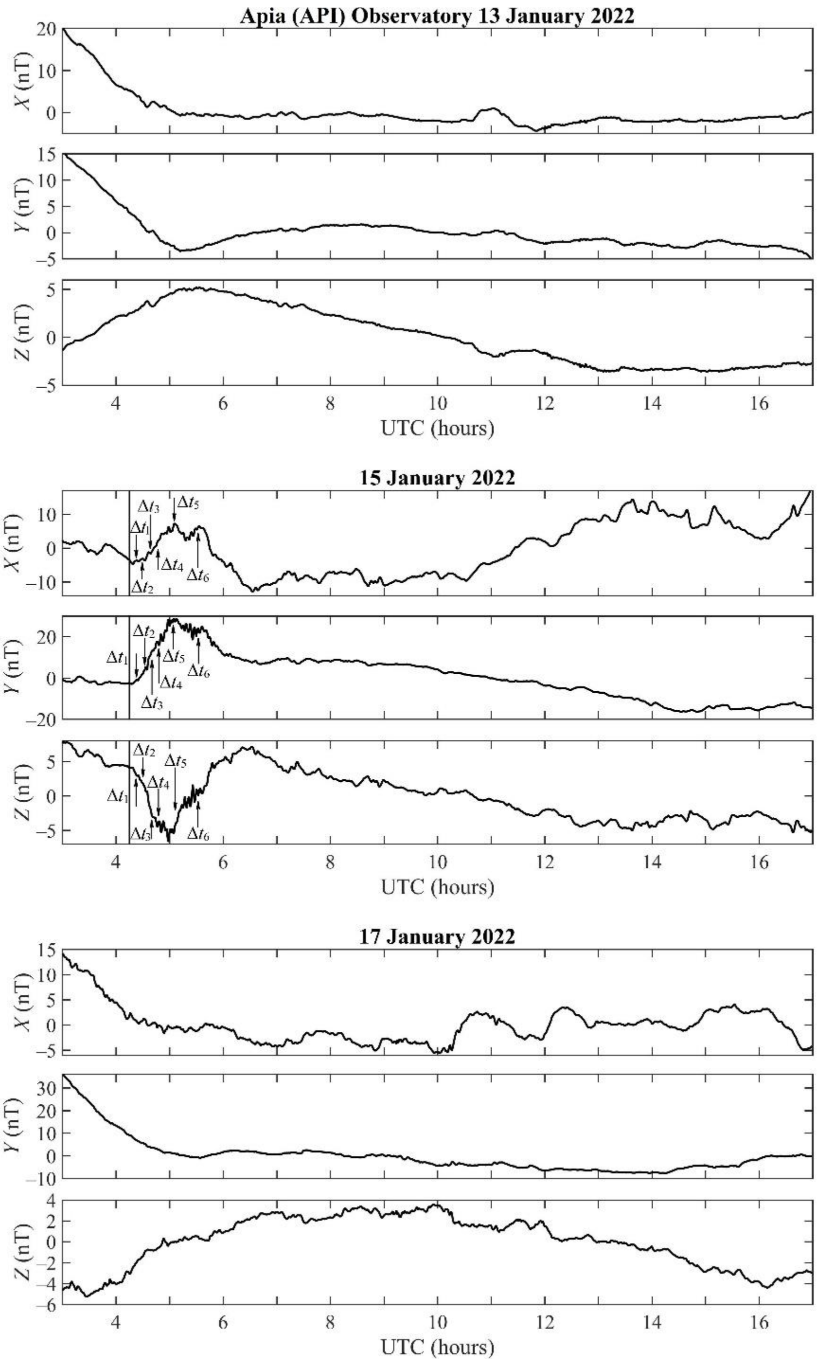


**Figure 2: UTC variations of the northward, *X*, eastward, *Y*, and vertical, *Z*, components of the geomagnetic field at the API station during 15 January 2022, the day of the volcanic explosion, and during the days used as a quiet time reference. The vertical line marks the moment of the most powerful explosion. Arrows indicate possible moments of the onset of the magnetic field response.**

https://doi.org/10.5194/angeo-2023-27
Preprint. Discussion started: 16 August 2023

Annales Geophysicae Discussions Open Access EGU

158 Table 3. Time delays and apparent speeds of disturbances in the geomagnetic field.

| Station | $\Delta t_1$ (min) | $v'_1$ (m/s) | $\Delta t_2$ (min) | $v'_2$ (m/s) | $\Delta t_3$ (min) | $v'_3$ (m/s) | $\Delta t_4$ (min) | $v'_4$ (m/s) | $\Delta t_5$ (min) | $v'_5$ (m/s) | $\Delta t_6$ (min) | $v'_6$ (m/s) |
|---|---|---|---|---|---|---|---|---|---|---|---|---|
| API | 8.5 | 4,000 | 14 | 1,560 | 19 | 1,000 | 33 | 500 | 50 | 311 | 75 | 200 |
| PPT | 16 | 4,100 | 37 | 1,420 | 50 | 1,011 | 96 | 500 | 150 | 314 | 235 | 198 |
| EYR | 17 | 3,875 | 38 | 1,410 | 50 | 1,033 | 97 | 505 | 155 | 310 | 240 | 200 |
| CNB | 21 | 4,000 | 47 | 1,500 | 68 | 1,006 | 130 | 507 | 208 | 312 | 322 | 200 |
| CTA | 22 | 3,900 | 49 | 1,510 | 71 | 1,008 | 137 | 504 | 217 | 314 | 338 | 200 |
| MCQ | 23 | 4,030 | 53 | 1,510 | 77 | 1,007 | 150 | 500 | 237 | 313 | 368 | 200 |
| HON | 26 | 4,000 | 61 | 1,490 | 89 | 1,000 | 173 | 498 | 272 | 313 | 424 | 200 |
| ASP | 27 | 3,950 | 63 | 1,500 | 92 | 1,000 | 185 | 482 | 282 | 313 | 440 | 200 |
| KDU | 28 | 4,060 | 67 | 1,500 | 98 | 1,004 | 190 | 505 | 305 | 311 | 475 | 199 |
| IPM | 33 | 3,970 | 79 | 1,500 | 115 | 1,011 | 215 | 530 | 360 | 313 | 565 | 199 |
| GNG | 34 | 4,000 | 82 | 1,500 | 119 | 1,007 | 235 | 500 | 372 | 312 | 580 | 200 |
| LRM | 35 | 4,018 | 85 | 1,500 | 125 | 1,000 | 245 | 500 | 390 | 313 | 615 | 198 |
| KAK | 38 | 3,967 | 90 | 1,540 | 135 | 1,007 | 260 | 513 | 490 | 315 | 645 | 204 |
| KNY | 39 | 3,988 | 95 | 1,507 | 140 | 1,004 | 270 | 512 | 435 | 315 | 685 | 199 |
| MMB | 39.5 | 3,993 | 97 | 1,497 | 143 | 998 | 273 | 514 | 442 | 315 | 690 | 201 |
| SHU | 40 | 4,070 | 100 | 1,501 | 147 | 1,004 | 285 | 509 | 460 | 313 | 720 | 199 |
| DLT | 43 | 3,976 | 106 | 1,501 | 156 | 1,001 | 305 | 504 | 488 | 313 | 760 | 200 |
| CKI | 44 | 3,978 | 110 | 1,477 | 160 | 1,001 | 310 | 509 | 500 | 313 | 780 | 200 |
| GAN | 56 | 3,990 | 140 | 1,507 | 208 | 1,002 | 410 | 502 | 660 | 311 | 1,020 | 200 |

https://doi.org/10.5194/angeo-2023-27
Preprint. Discussion started: 16 August 2023

Annales Geophysicae Discussions

*PPT Station.* On 13 and 17 January 2022, used as a quiet time reference, the strength of the *X*-component showed variations from about (–4)–(–5) nT to 2–5 nT (Figure 3) throughout the entire 03:00–17:00 UTC period, whereas the *Y*-component increased from (–6)–(–7) nT to 7–8 nT over the 03:00–05:00 UTC period and afterwards exhibited fluctuations within the 2–3-nT limits, gradually decreasing from ~0 nT to (–15)–(–23) nT. On 13 January 2022, the *Z*-component exhibited undulating oscillation during the 03:00 to ~10:00 UTC period followed by a gradual decrease from ~0 to –10 nT, whereas on 17 January 2022, it showed a broad maximum of 8 nT near ~04:00 UTC followed by a gradual decrease to a minimum of –5.1 nT at ~10:30 UTC and later by oscillations with an amplitude of ~1 nT around the trend changing in the –5.1- to 0-nT range.

On the day of the volcanic explosion, the non-monotonousness in the magnitude of all components increased, the fluctuations of the components also somewhat increased, while the trend substantially smoothed in all components. The magnitude of the *X*-component increased from –10 nT to 20 nT, the value of the *Y*-component decreased from 15 nT to –20 nT, and of the *Z*-component decreased from 10 nT to –5 nT. In addition, six groups of disturbances appeared with time delays of $\Delta t_1 \approx 16$ min, $\Delta t_2 \approx 37$ min, $\Delta t_3 \approx 50$ min, $\Delta t_4 \approx 96$ min, $\Delta t_5 \approx 150$ min, and $\Delta t_6 \approx 235$ min (see Figure 3). The greatest disturbances (up to 10 nT) occurred after 14:00 UTC in the *X* component.

*EYR Station.* On 13 January 2022, the strength of the *X*-component increased, fluctuating, from –5 nT to 10 nT, and then decreased from 10 nT to –3 nT (Figure 4). Since 06:00 UTC, the magnitude of the *X*-component fluctuated around the 2-nT value. The strength of the *Y*-component first showed a decrease from 12 nT to ~0 nT during the 03:30–05:00 UTC period, then it fluctuated around ~0 nT, and afterwards its value was observed to decrease to –(5–10) nT. The magnitude of the *Z*-component decreased from ~8 nT to 0 nT and fluctuated around 0 nT afterwards. On 17 January 2022, the magnitude of the *X*-component was fluctuating around 0 nT, with excursions attaining 6–7 nT, while the magnitude of the *Y*-component was decreasing, fluctuating, from ~20 nT to –10 nT. At the same time, the strength of the *Z*-component decreased from 7–8 nT to –10 nT, and then it increased, noticeably fluctuating, from –10 nT to 7 nT.

On the day the volcanic explosion occurred, the number of groups of disturbances was observed to attain six. The most pronounced disturbances were negative geomagnetic bay disturbances with time delays of $\tau_X \approx 86$ min, $\tau_Y \approx 51$ min and $\tau_Z \approx 51$ min. The drops in the *X*-, *Y*-, and *Z*-components attained –39 nT, –27 nT, and –22 nT, respectively. The drops in the *X*-, *Y*-, and *Z*-component strengths were followed up by increases of ~38 nT, 30 nT, and 30 nT, respectively. The amplitudes of other disturbances usually did not exceed a few nanoteslas, and they arrived with time delays of $\Delta t_1 \approx 15$ min, $\Delta t_2 \approx 38$ min, $\Delta t_3 \approx 50$ min, $\Delta t_4 \approx 97$ min, $\Delta t_5 \approx 155$ min, and $\Delta t_6 \approx 240$ min (see Table 3).

https://doi.org/10.5194/angeo-2023-27
Preprint. Discussion started: 16 August 2023


Annales Geophysicae Discussions

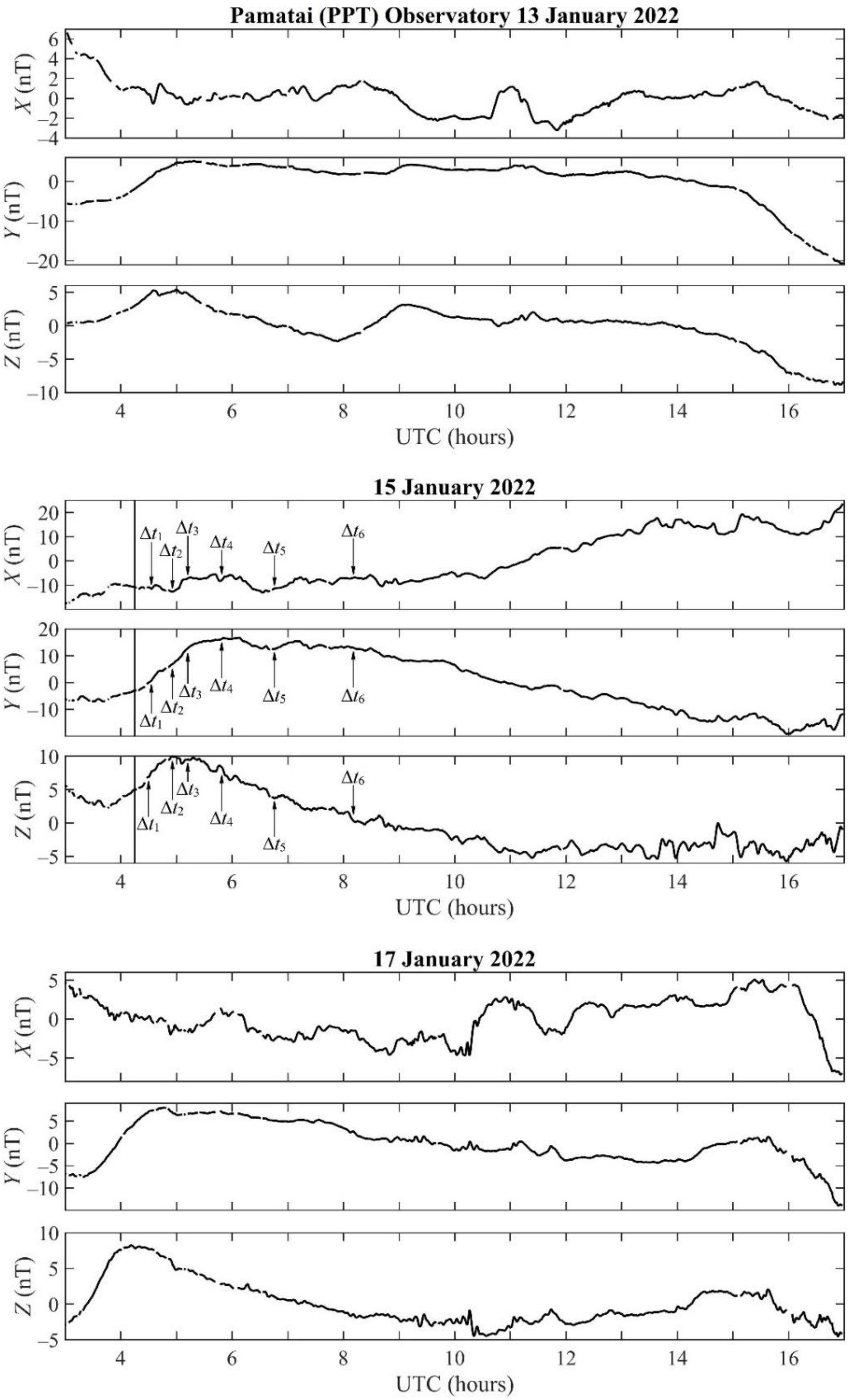


187

188 **Figure 3: Same as in Figure 2 but for the PPT station.**

https://doi.org/10.5194/angeo-2023-27
Preprint. Discussion started: 16 August 2023


Annales Geophysicae
Discussions
Open Access
EGU

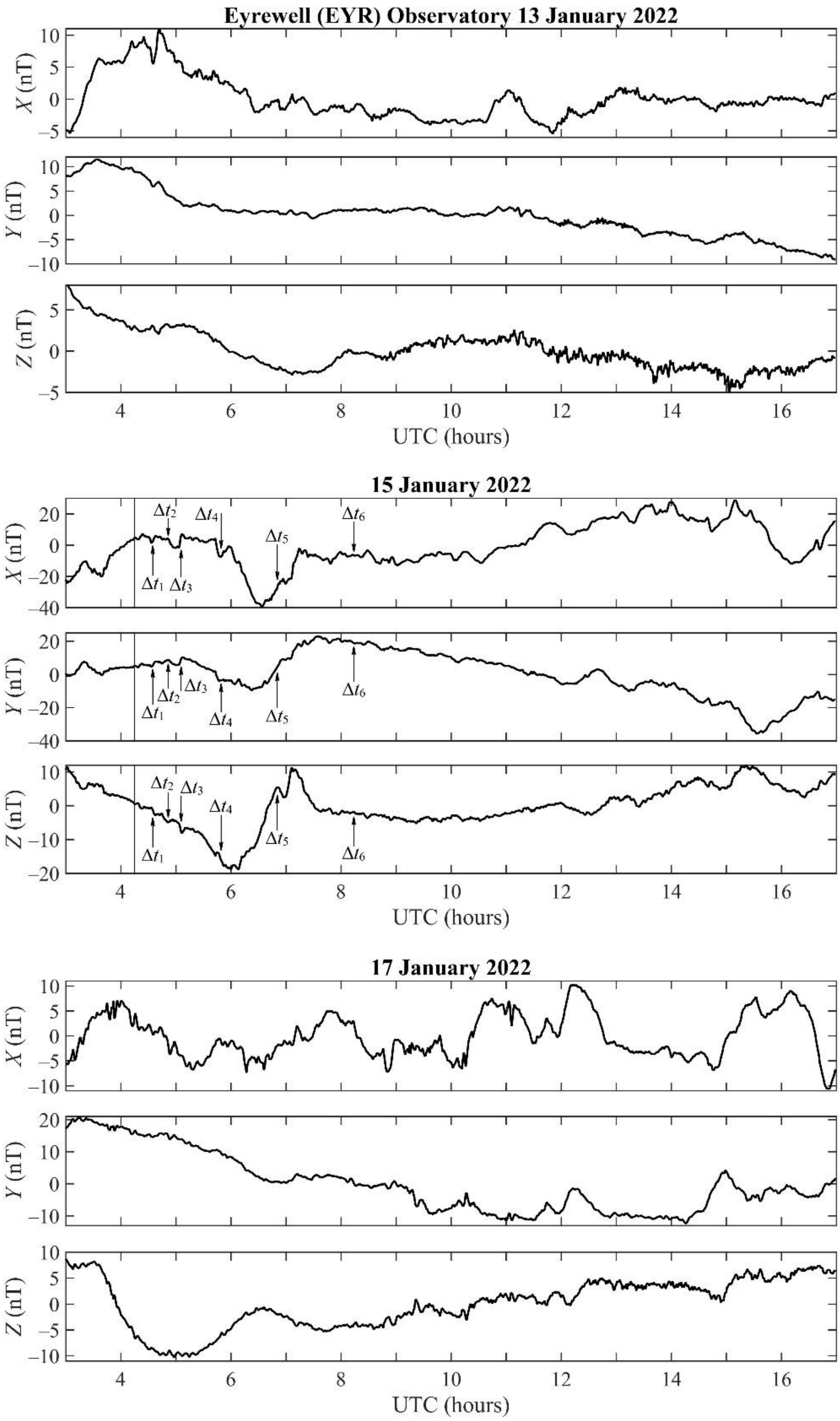


**Figure 4: Same as in Figure 2 but for the EYR station.**

https://doi.org/10.5194/angeo-2023-27
Preprint. Discussion started: 16 August 2023


Annales Geophysicae Discussions

*CNB Station.* On 13 January 2022, the fluctuations in the magnitude of all components did not exceed 1–4 nT (Figure 5). The strength of the *Y*-component showed a decrease from ~17 nT to –5 nT. The *Z*-component was observed to drop from 4 nT to –7 nT over the 03:00–05:00 UTC period, and then its magnitude showed fluctuations around 1 nT. On 17 January 2022, the strength of the *X*-component gradually increased from –10 nT to 10 nT, fluctuating within the ±(5–7)-nT limits, while the magnitude of the *Y*-component decreased from 27 nT to –10 nT. The strength of the *Z*-component increased from –12 nT to 7 nT first, and then fluctuated within the ±(3–4)-nT limits.

During the course of the day the volcanic explosion occurred, the trend $\overline{X}$ first increased from –10 nT to 10 nT, then it decreased from 10 nT to –10 nT, and once again increased from –10 nT to 30 nT, while the magnitude of fluctuations was observed to be ±(3–5) nT. The trend $\overline{Y}$ first decreased from 16 nT to –40 nT, then it increased from –40 nT to 28 nT, and once again decreased from 28 nT to –30 nT. The trend $\overline{Z}$ first decreased from –8 nT to –13 nT, then it increased from –13 nT to 14 nT, and once again decreased from 14 nT to –5 nT, which was followed by an increase in $\overline{Z}$ from –5 nT to 15 nT. The variations with amplitude of a few nanotesla were superimposed on the slow trend in all components.

*CTA Station.* On the days used as a quiet time reference, the magnitudes of all components exhibited relatively small fluctuations (Figure 6) except for the variations in the *X*-component on 17 January 2022 when its strength showed fluctuations within the ±5-nT limits while the trend $\overline{X}$ increased from –10 nT to 5 nT. Instead, the trend $\overline{Y}$ decreased from 25 nT to approximately –10 nT, and the trend $\overline{Z}$ from 13 nT to –5 nT. On 13 January 2022, the trend $\overline{X}$ decreased from 12 nT to –5 nT over the 03:00–05:00 UTC period and then remained at this level. The trend $\overline{Y}$ decreased from 7 nT to –4 nT from 03:00 UTC to 07:00UTC, then increased to 2 nT, and afterwards gradually decreased from 2 nT to –5 nT. The trend $\overline{Z}$ sharply decreased from 8 nT to –2 nT over the 03:00 UTC to 07:00 UTC period, and then it showed fluctuations around 0 nT. During 13 and 17 January 2022 used as a quiet time reference, synchronous geomagnetic bay disturbances were absent (Figure 6).

The magnitude of fluctuations in all components considerably increased on 15 January 2022. The trend $\overline{X}$ increased from –15 nT to 20 nT. The *Y*-component, in addition to fluctuations, exhibited a deep drop from ~15 nT to –45 nT that occurred from 05:45 UTC to 08:30 UTC (see Figure 6). The *Z*-component also showed a drop from ~0 nT to –13 nT during the 05:20–07:15 UTC period, followed by a surge from –13 nT to ~23 nT. In addition, the disturbances appeared in all components with time delays of 22 min, 49 min, 71 min, 137 min, 217 min, and 338 min (see Figure 6).

https://doi.org/10.5194/angeo-2023-27
Preprint. Discussion started: 16 August 2023


Annales Geophysicae Discussions
Open Access
EGU

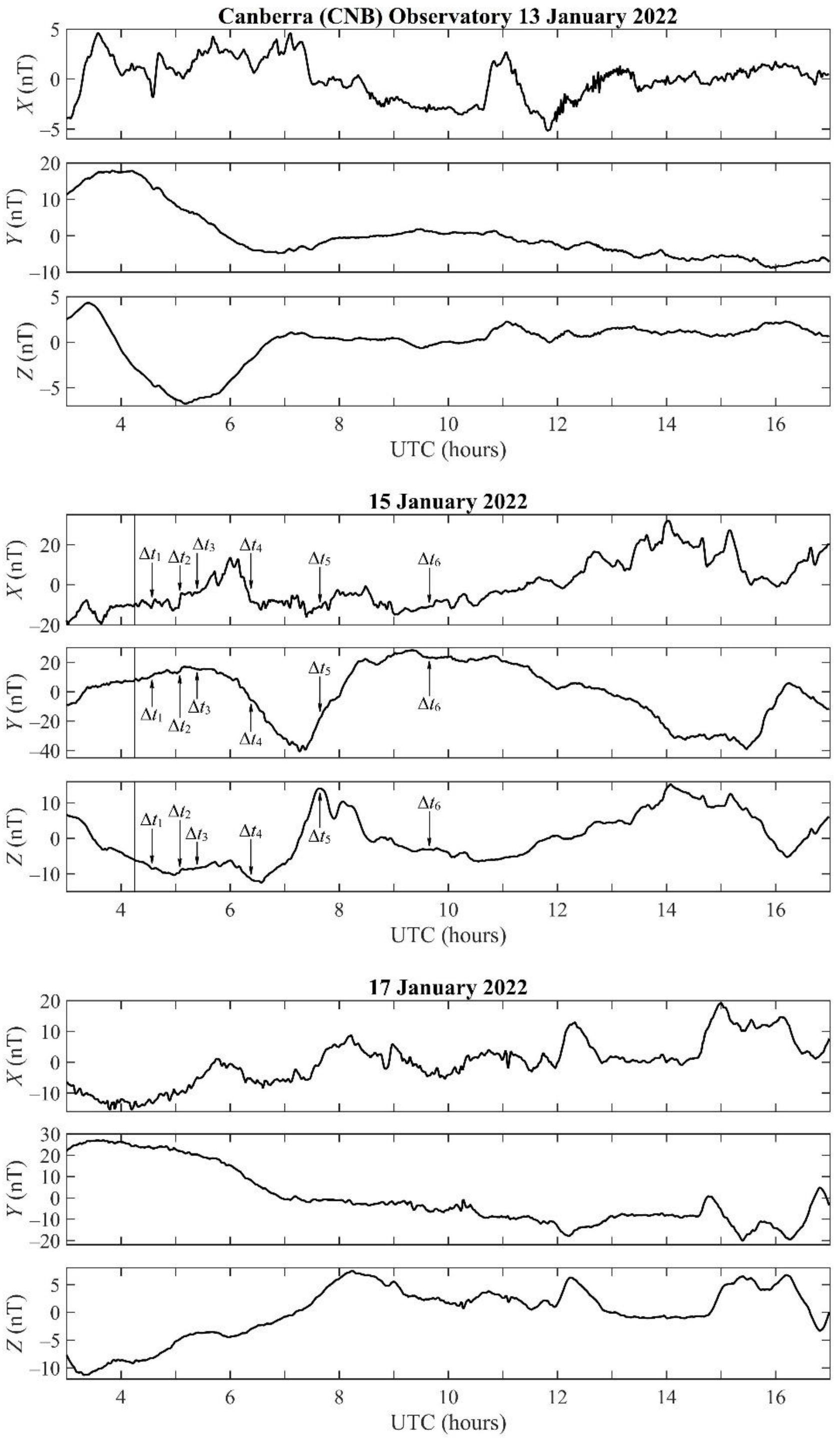


217
218 **Figure 5: Same as in Figure 2 but for the CNB station.**

https://doi.org/10.5194/angeo-2023-27
Preprint. Discussion started: 16 August 2023


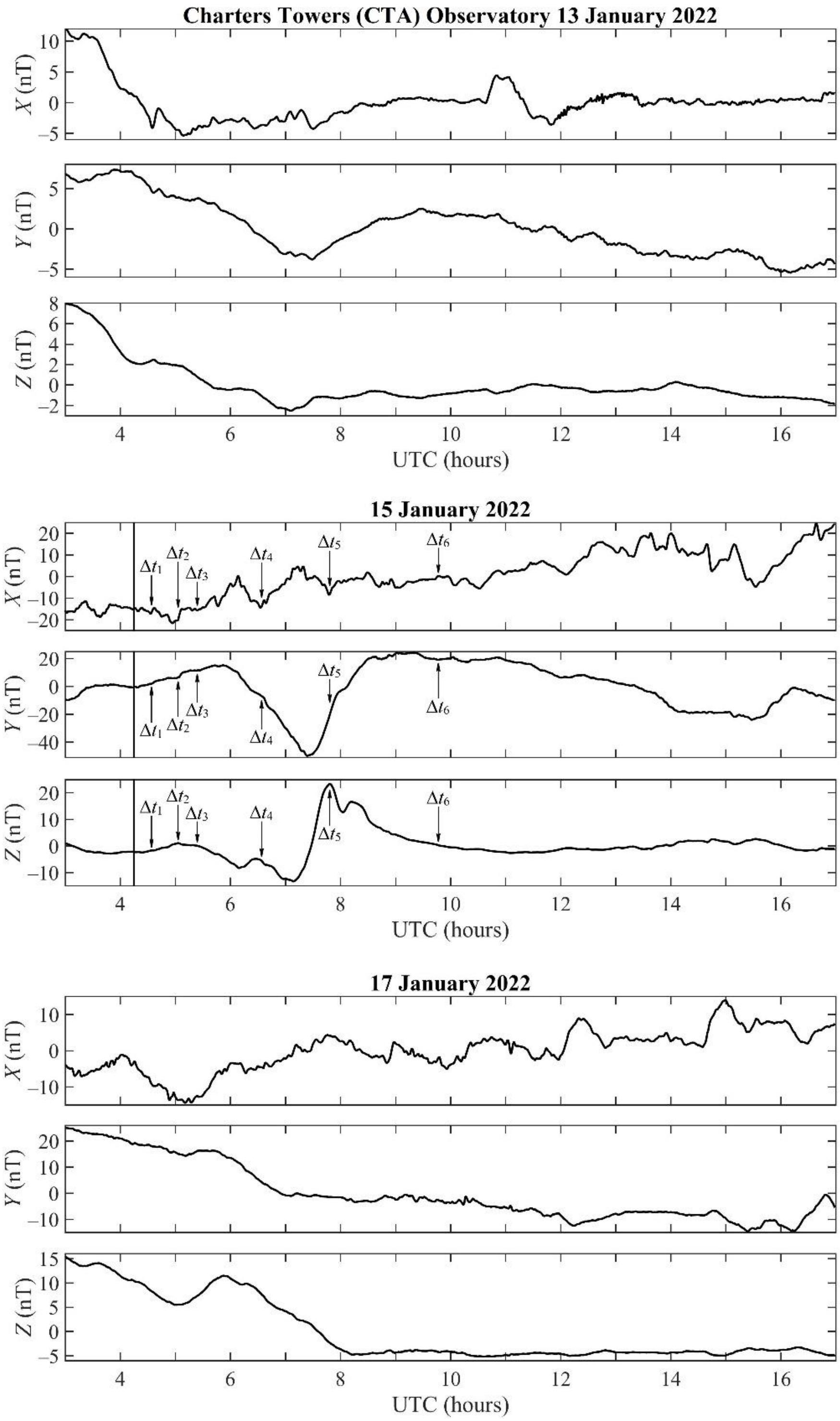


**Figure 6: Same as in Figure 2 but for the CTA station.**

https://doi.org/10.5194/angeo-2023-27
Preprint. Discussion started: 16 August 2023


Annales Geophysicae Discussions Open Access EGU

*MCQ Station.* On 13 January 2022, $X(t)$, $Y(t)$, and $Z(t)$ components showed variations in the trend not exceeding 20 nT (Figure 7), as well as fluctuations within the ±3-nT range. On 17 January 2022, the strengths of all components showed small variations up to 10:00 UTC, whereas the variations increased to 100–200 nT after 10:00 UTC.

On the day the volcanic explosion occurred, all components exhibited relatively small variations before 11:00 UTC, whereas they showed an increase of up to 300–400 nT after 11:00 UTC. Approximately from 06:00 UTC to 08:00–09:00 UTC, the strengths of the *X*-, *Y*-, and *Z*-component decreased by 80 nT, 40 nT, and 30 nT, respectively. Such a perturbation pertains to a bay disturbance. In addition, except for the bay disturbance, quasi-periodic disturbances occurred with strengths of 1–10 nT and $T \approx$ 5–10-min periods.

*HON Station.* On 13 January 2022, the *X* component exhibited weak fluctuations within the ±1 nT limits from 00:00 UTC to 10:00 UTC (Figure 8). After 10:00 UTC, the level of variability noticeably increased. The strength of the *Y* component displayed a rise from –4 nT to 6 nT over the 00:00–04:00 UTC period, followed by a gradual decrease to 0 nT at 12:00, and the trend continued to decrease later. Throughout the 00:00–04:00 UTC period, the magnitude of the *Z* component showed first an increase from –3 nT to 1.3 nT, and then it decreased, fluctuating, from 1.3 nT to –2 nT. On 17 January 2022, all components showed insignificant (less than 1 nT) fluctuations from 00:00 UTC to 10:00 UTC. After 10:00 UTC, the magnitude of the fluctuations increased to ±3 nT.

On 15 January 2022, the *X* component exhibited fluctuations within the ±(5–7) nT limits, and the fluctuations in the strength of the *Y* component was noticeable enough (up to ±(2–4) nT) as well. The *Z* component also showed a significant enhancement in fluctuations after the volcanic explosion, while all geomagnetic field components exhibited several groups of disturbance from 04:30 UTC to 12:00 UTC.

*ASP Station.* On 13 January 2022 used as a quiet time reference, the trend $\overline{X}$ first decreased from ~15 nT to –(5–0) nT, and then it remained at a level of 0 nT (Figure 9). The trend $\overline{Y}$ decreased from ~8 nT to –5 nT, whereas the trend $\overline{Z}$ first sharply decreased from 13 nT to –3 nT, and then it exhibited variations between –3 nT and –1 nT. The strengths of fluctuations in all components usually did not exceed 1–2 nT. On 17 January 2022 used as a quiet time reference interval, the trend $\overline{X}$ exhibited insignificant changes, and the strength of fluctuations did not exceed ±(3–5) nT. The trend $\overline{Y}$ decreased from 27 nT to –21 nT, and its strength showed fluctuations attaining ±(8–10) nT. The trend $\overline{Z}$ first sharply decreased from 19 nT to –5 nT, and then $\overline{Z} \approx -4$ nT; the magnitude of fluctuations did not exceed ±1 nT.

During the day the volcanic explosion occurred, all components of the geomagnetic field experienced geomagnetic bay disturbances that were superimposed on fluctuations with strengths of up to 4–5 nT. The trend $\overline{X}$ exhibited a drop from 0 nT to –15 nT, whereas the trend $\overline{Y}$ showed a considerably greater drop, from 12 nT to –40 nT, of almost 4 h temporal duration; a powerful surge from –40 nT to 20 nT of 5.5 h duration followed afterwards. The trend $\overline{Z}$ first increased from –10 nT to –2 nT, then decreased from –2 nT to –10 nT, and increased from –10 nT to 22 nT afterwards; this surge in the trend $\overline{Z}$ was followed by a decrease to 0–5 nT.

https://doi.org/10.5194/angeo-2023-27
Preprint. Discussion started: 16 August 2023


Annales Geophysicae
Discussions
Open Access
EGU

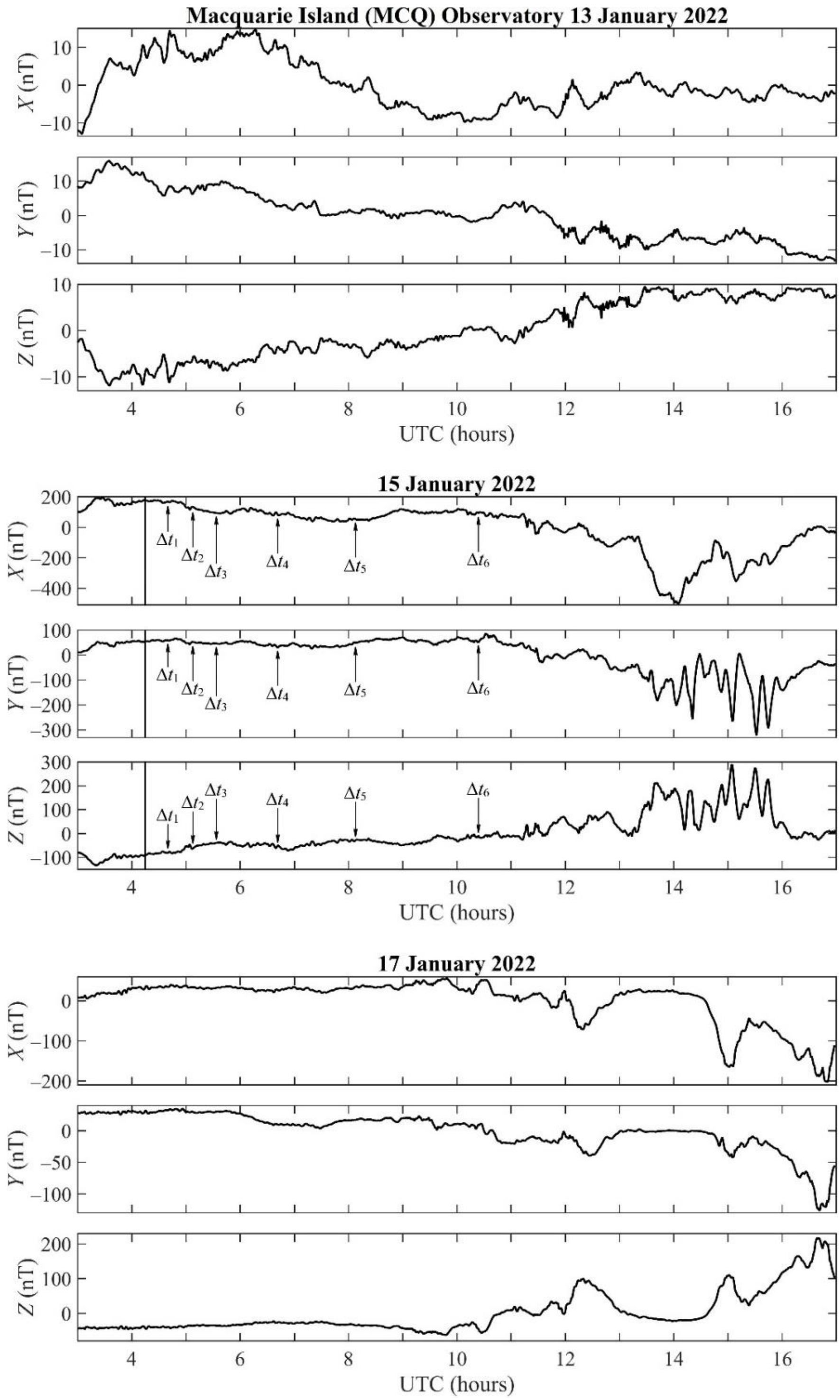


253
254 **Figure 7: Same as in Figure 2 but for the MCQ station.**

https://doi.org/10.5194/angeo-2023-27
Preprint. Discussion started: 16 August 2023

Annales Geophysicae Discussions

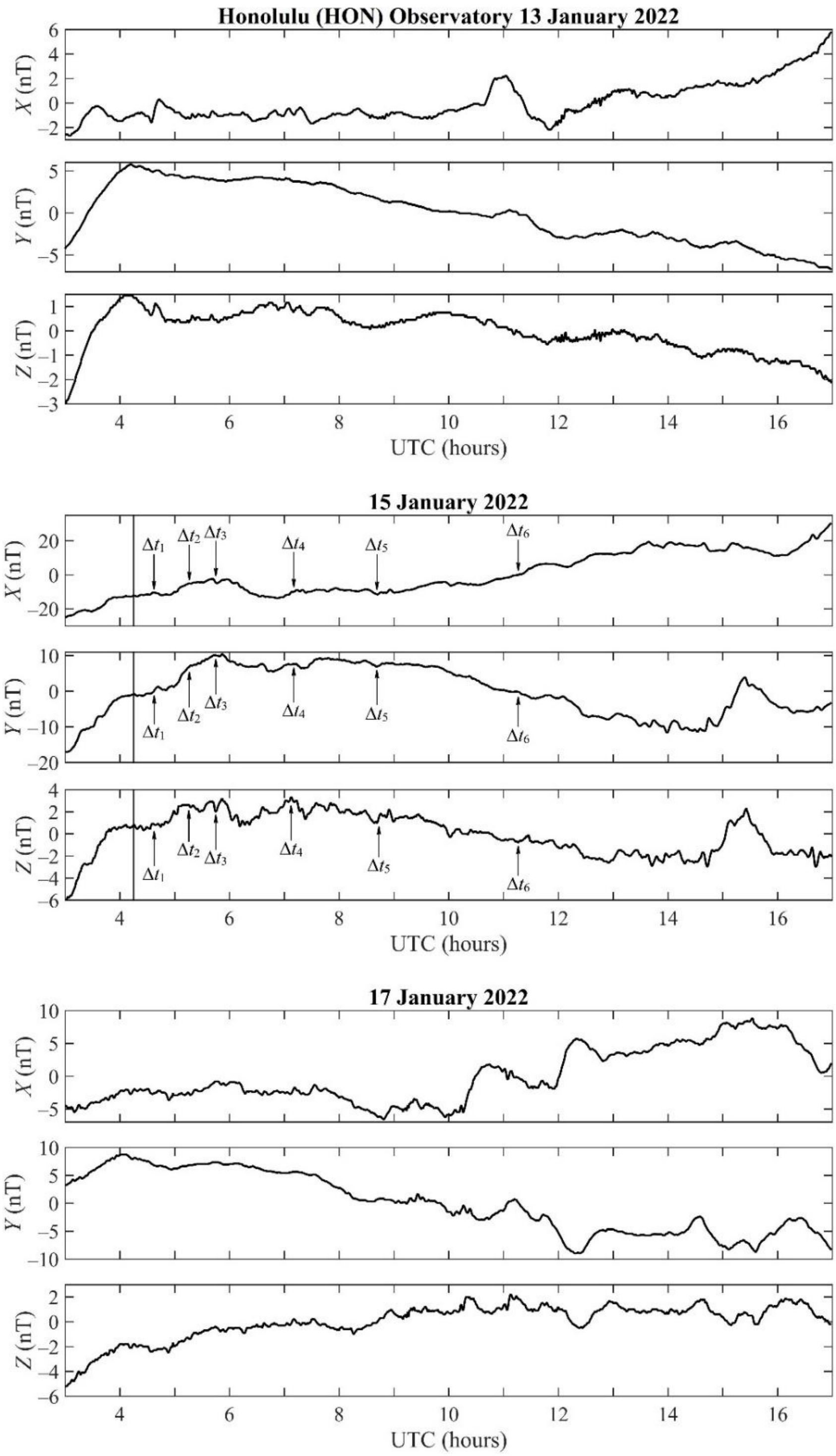


**Figure 8: Same as in Figure 2 but for the HON station.**

https://doi.org/10.5194/angeo-2023-27
Preprint. Discussion started: 16 August 2023

Annales Geophysicae
Discussions
Open Access

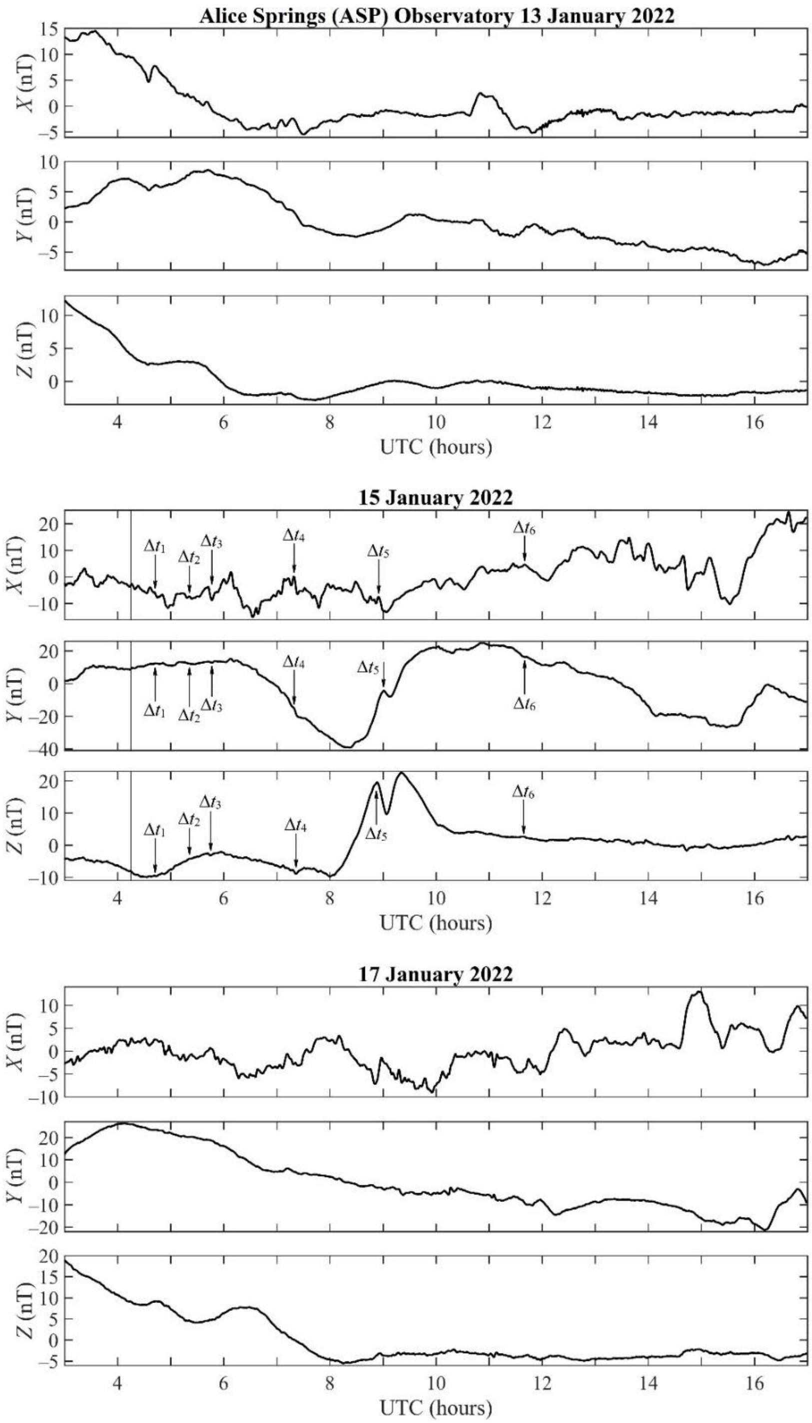


**Figure 9: Same as in Figure 2 but for the ASP station.**

https://doi.org/10.5194/angeo-2023-27
Preprint. Discussion started: 16 August 2023


*KDU Station.* On 13 January 2022, the trend $\overline{X}$ first sharply decreased from ~27 nT to –5 nT, and then it showed fluctuations around a strength of –5 nT (Figure 10). At the same time, the trend $\overline{Y}$ gradually decreased from 2–3 nT to –4 nT, while the trend $\overline{Z}$ first (up to 06:30 UTC) increased to 11 nT, then sharply decreased to –5 nT and did not change afterwards. During 17 January 2022, the behavior of the trends $\overline{X}$ and $\overline{Y}$ was qualitatively analogous to their behavior observed on 13 January 2022; however, fluctuations in the strength increased to 2–4 nT. The trend $\overline{Z}$, fluctuating, decreased from approximately 14 nT to –5 nT.

On the day the volcanic explosion occurred, the trend $\overline{X}$ first decreased, fluctuating, from –7 nT to –15 nT, next it increased from –15 nT to 10 nT before ~14:00 UTC, and then a drop was observed to occur to –10 nT over the 14:00–15:30 UTC period. The trend $\overline{Y}$ first increased from –3 nT to 8 nT, next it decreased from 8 nT to –23 nT, then it increased from –23 nT to 20–22 nT, and finally it gradually decreased from 20–22 nT to –18 nT. The trend $\overline{Z}$ first increased from ~3 nT to 9 nT, then it decreased from 9 nT to –8 nT, and once again increased from –8 nT to 13 nT. After this peak, the value of $\overline{Z}$ was observed to gradually decrease from 13 nT to –5 nT. Variations with amplitudes of a few nanotesla were superimposed on the relatively smooth changes in all components.

*IPM Station.* On 13 January 2022 used as a quiet time reference, the magnitude of all components before 11:00–12:00 UTC varied within the 5–7-nT limits (Figure 11). Quasi-periodic variations were virtually absent. During 17 January 2022 up to 12:00 UTC, the variations in *X*-, *Y*-, and *Z*-components did not exceed 3–5 nT.

On 15 January 2022, the day the volcanic explosion occurred, insignificant bay reductions of only (4–8) nT in the magnitudes of all components were observed to appear with time delays of 120–125 min and durations of 210–230 min, whereas quasi-periodic disturbances were virtually absent.

*GNG Station.* On 13 January 2022, used as a quiet time reference, the trend $\overline{X}$ first sharply decreased from 20 nT to –5 nT and then fluctuated around –5 nT (Figure 12). The trend $\overline{Y}$, fluctuating within the ±(3–4)-nT limits, gradually decreased from 12 nT to –5 nT. Over the 03:00–09:00 UTC period, the trend $\overline{Z}$ substantially sharply decreased from 25 nT to –8 nT, next it remained almost constant. On 17 January 2022, also used as a quiet time reference, the trend $\overline{X}$ gradually increased from –12 nT to 10 nT, while the strength of the *X*-component showed fluctuations within the ±(4–10)-nT limits. The trend $\overline{Y}$ first increased to 30 nT, and then gradually decreased from 30 nT to –20 nT showing fluctuations sometimes attaining ±5–10 nT. The trend $\overline{Z}$ increased to 38 nT by 05:30 UTC, then decreased to –17 nT by 12:00 UTC, and later almost did not change; the amplitude showed fluctuations within the ±4–5-nT limits after 12:00 UTC.

Throughout the day the volcanic explosion occurred, all components showed variations qualitatively different from those observed over a quiet time period. Approximately since 06:00 UTC, all components reduced their strengths by 20–50 nT during 2–3 h. Next, their strengths increased by 15–40 nT over an almost 2-h interval. All components exhibited 5–9-nT variations superimposed on the slow changes.

https://doi.org/10.5194/angeo-2023-27
Preprint. Discussion started: 16 August 2023


Annales Geophysicae
Discussions
Open Access

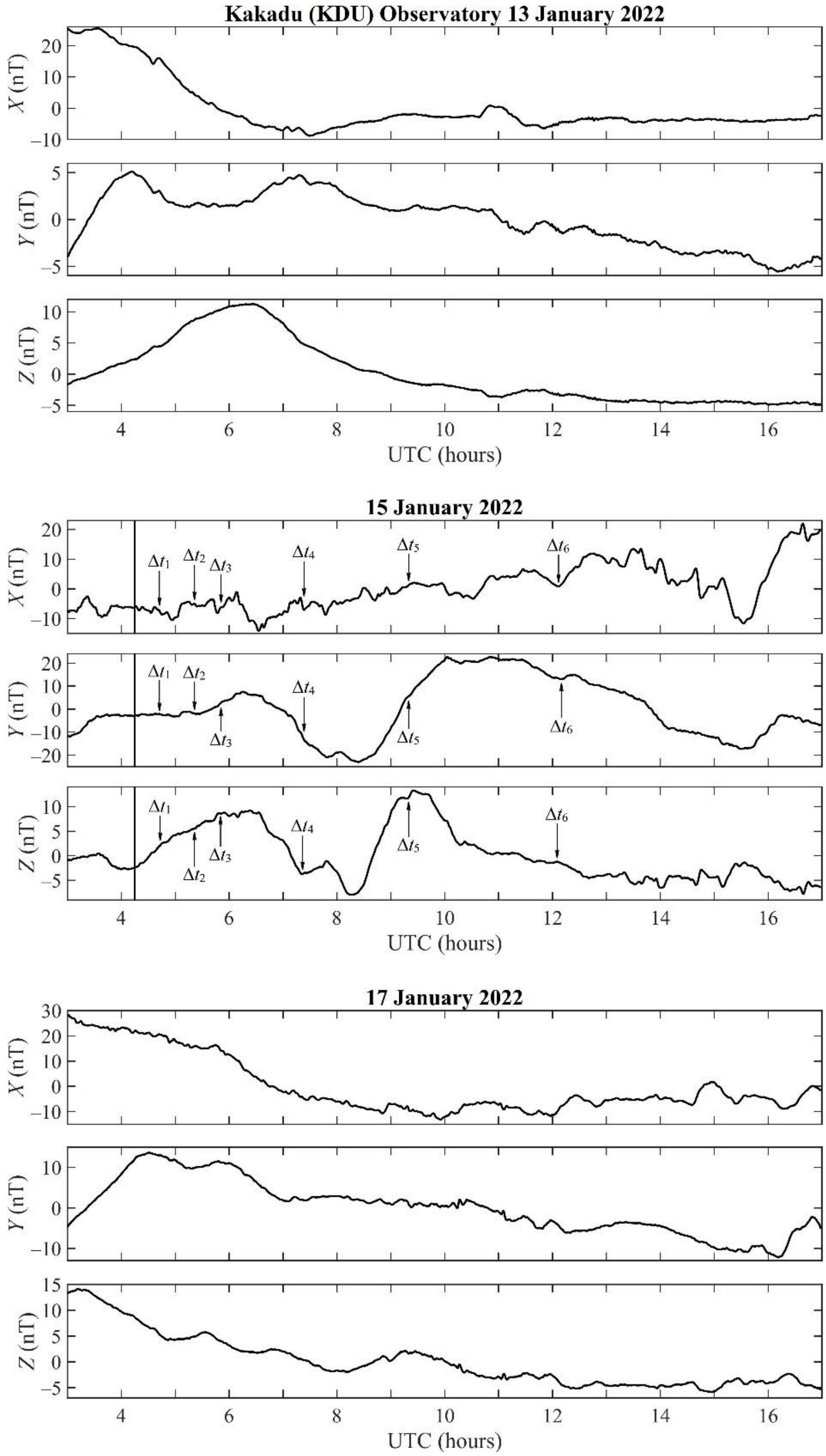


**Figure 10: Same as in Figure 2 but for the KDU Station.**

https://doi.org/10.5194/angeo-2023-27
Preprint. Discussion started: 16 August 2023




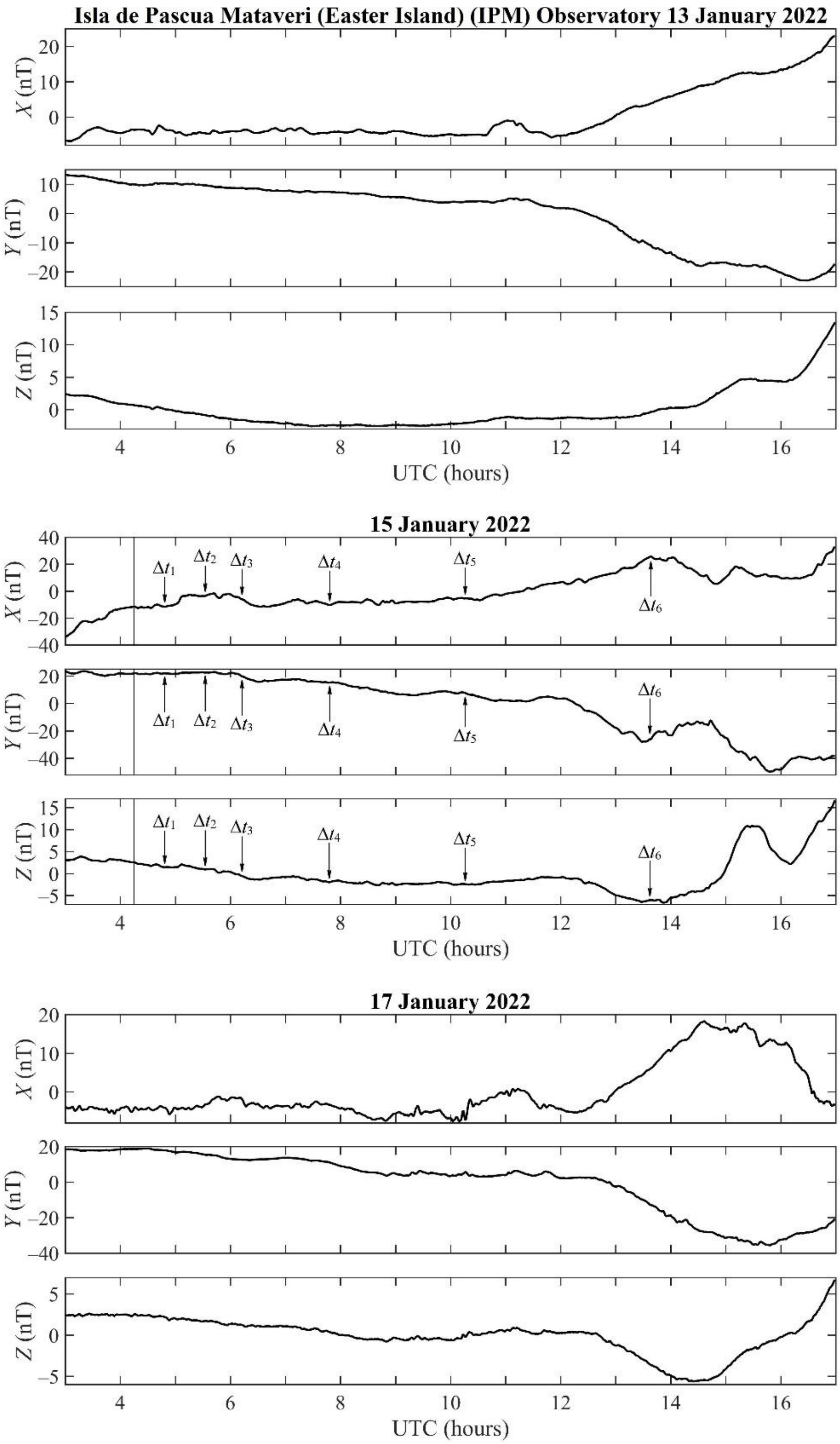


292

293 **Figure 11: Same as in Figure 2 but for the IPM Station.**

https://doi.org/10.5194/angeo-2023-27
Preprint. Discussion started: 16 August 2023


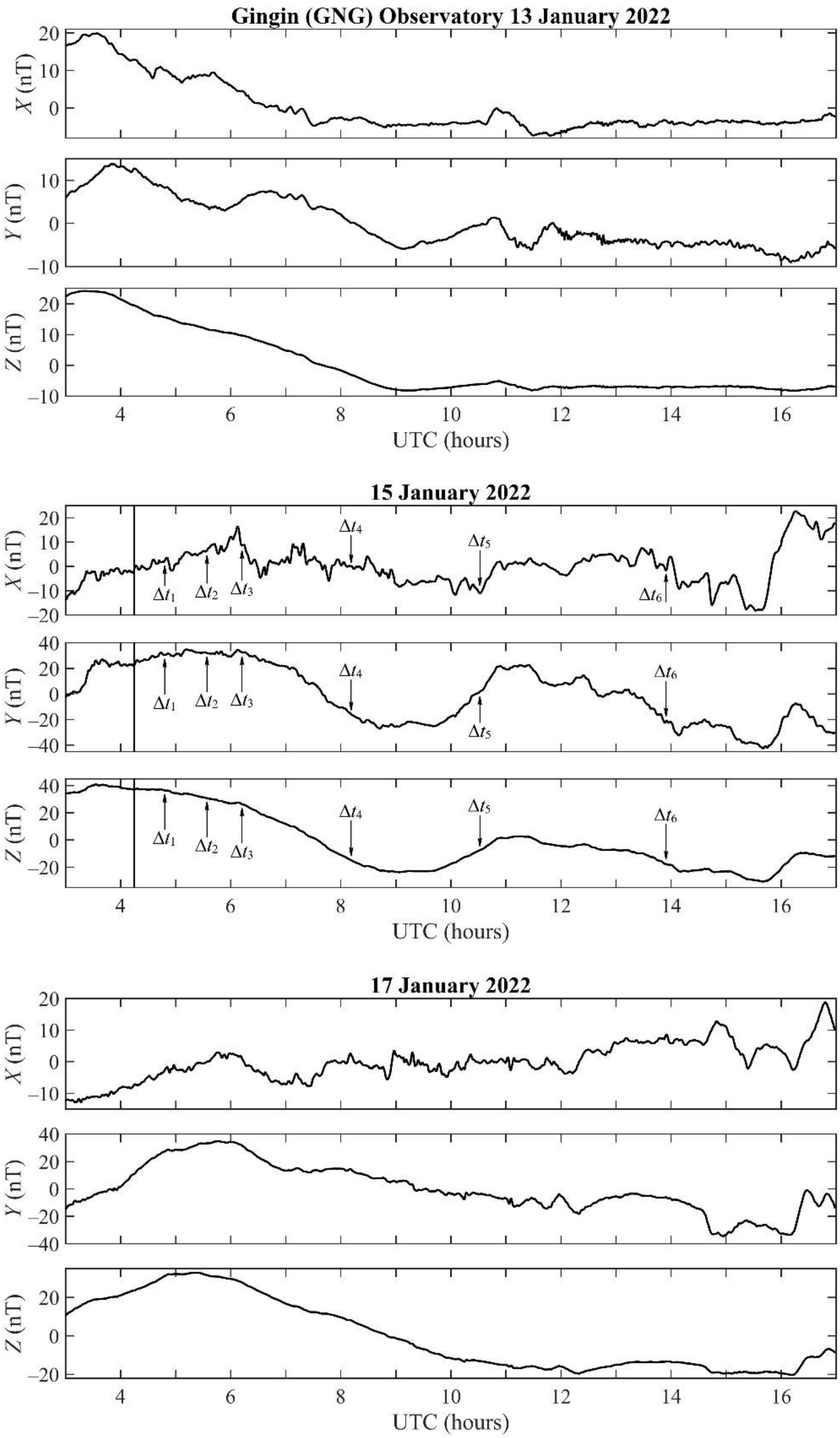


**Figure 12: Same as in Figure 2 but for the GNG Station.**

https://doi.org/10.5194/angeo-2023-27
Preprint. Discussion started: 16 August 2023




*LRM Station.* On 13 January 2022, the trend $\overline{X}$ nearly linearly decreased from 30 nT to –10 nT over the 03:30–08:30 UTC period, and later it changed insignificantly, while the trend $\overline{Y}$ showed variations not exceeding ~7–8 nT (Figure 13). The trend $\overline{Z}$ first showed fluctuations about the 7-nT strength level, and later about the –5-nT level. On 17 January 2022, the trend $\overline{X}$ showed fast fluctuations within the ±10-nT limits, while the trend itself first increased to 06:00 UTC, and then decreased from 14 nT to –10 nT before 10:00 UTC. The trend $\overline{Y}$ increased from –15 nT to 25 nT, and then decreased nonmonotonically to –20 nT, while the amplitude of fluctuations attained ±(5–6) nT. The trend $\overline{Z}$ decreased from 40 nT to –15 nT during the 04:00–10:00 UTC period and then fluctuated around –20 nT.

On 15 January 2022, the day the volcanic explosion occurred, the variations were observed to be substantially different. After exhibiting insignificant fluctuations from 03:00 UTC to 06:00 UTC, the trends decreased by approximately 40 nT. After this, the trends were observed to increase by 20–50 nT over a 1–2-h interval. The amplitudes showed fluctuations that did not exceed ±(3–4) nT.

*KAK Station.* On 13 January 2022, used as a quiet time reference, the trend $\overline{X}$ increased from –20 nT to 5 nT over the 03:00–08:00 UTC period, and then gradually decreased from 5 nT to 0 nT (Figure 14). The trend $\overline{Y}$ decreased to –19 nT by 05:00 UTC, after that it increased to 0 nT by 08:00 UTC and then remained essentially constant. The trend $\overline{Z}$ increased from –15 nT to 8 nT over the 03:00–06:00 UTC period, next it decreased from 7 nT to 0 nT from 07:00 UTC to 09:00 UTC, and then almost did not change. The magnitude of fluctuations in all components did not exceed ±1 nT. On 17 January 2022 used as a quiet time reference, the trend $\overline{X}$ increased from –10 nT to 5 nT, though a reduction in the dependence $\overline{X}(t)$ was observed to occur from 08:00 UTC to 15:00 UTC, and $\overline{X} \approx 6$ nT from 15:00 UTC to 17:00 UTC. The trend $\overline{Y}$ first decreased to –17 nT, and then increased to 5 nT. The trend $\overline{Z}$ increased to 2 nT by 06:40 UTC and dropped from 2 nT to –3 nT over the 06:40–12:00 UTC period. Then $\overline{Z} \approx 2$ nT. The amplitude showed fluctuations attaining 2–3 nT in every component.

During the course of the day the volcanic explosion occurred, the magnitude of fluctuations in every component increased noticeably. The trend $\overline{X}$, fluctuating, decreased from 6 nT to –7 nT from 06:00 UTC to 10:00 UTC. Next, it increased from –7 nT to 10 nT over a 3-h interval, and finally the trend decreased to –13 nT. The trend $\overline{Y}$ also first increased from –27 nT to –7 nT, then it decreased by less than 10 nT over a 1.5-h interval, after which the trend $\overline{Y}$ increased to 17 nT at 13:30 UTC. A clear quasi-periodic perturbation with a period of $T \approx$ 55–60 min and a strength of 4 nT was recorded from approximately 11:00 UTC to 14:00 UTC. Other disturbances had amplitudes of 1–1.5 nT. The trend $\overline{Z}$ showed fluctuations within the ±3-nT limits throughout the 03:00–07:00 UTC period, when the trend remained almost the same, next, from 07:00 UTC to 12:00 UTC, the trend decreased from 3 nT to –5 nT, and finally it increased. The fluctuations occurred with an amplitude of ~1 nT.

https://doi.org/10.5194/angeo-2023-27
Preprint. Discussion started: 16 August 2023


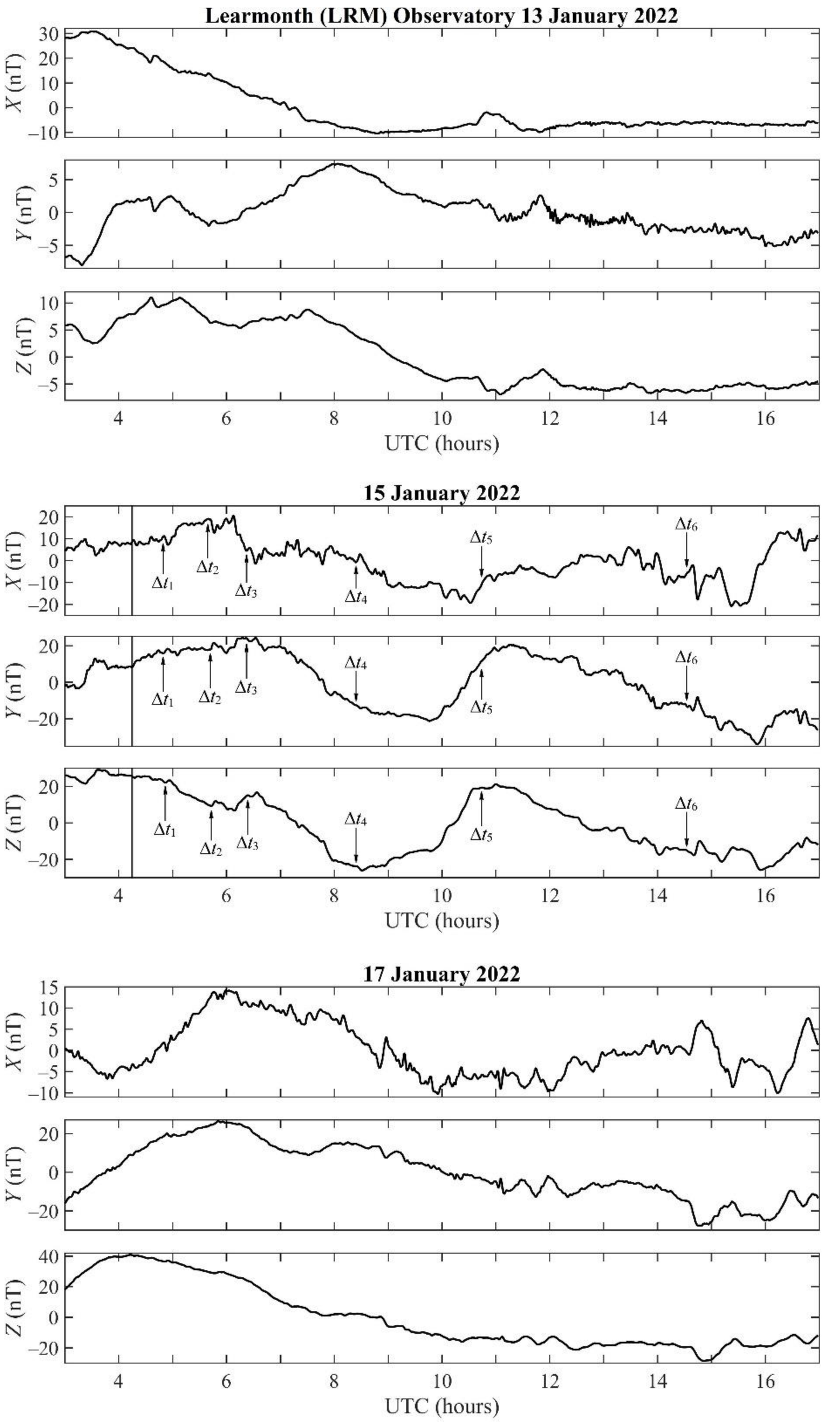


**Figure 13: Same as in Figure 2 but for the LRM Station.**

https://doi.org/10.5194/angeo-2023-27
Preprint. Discussion started: 16 August 2023


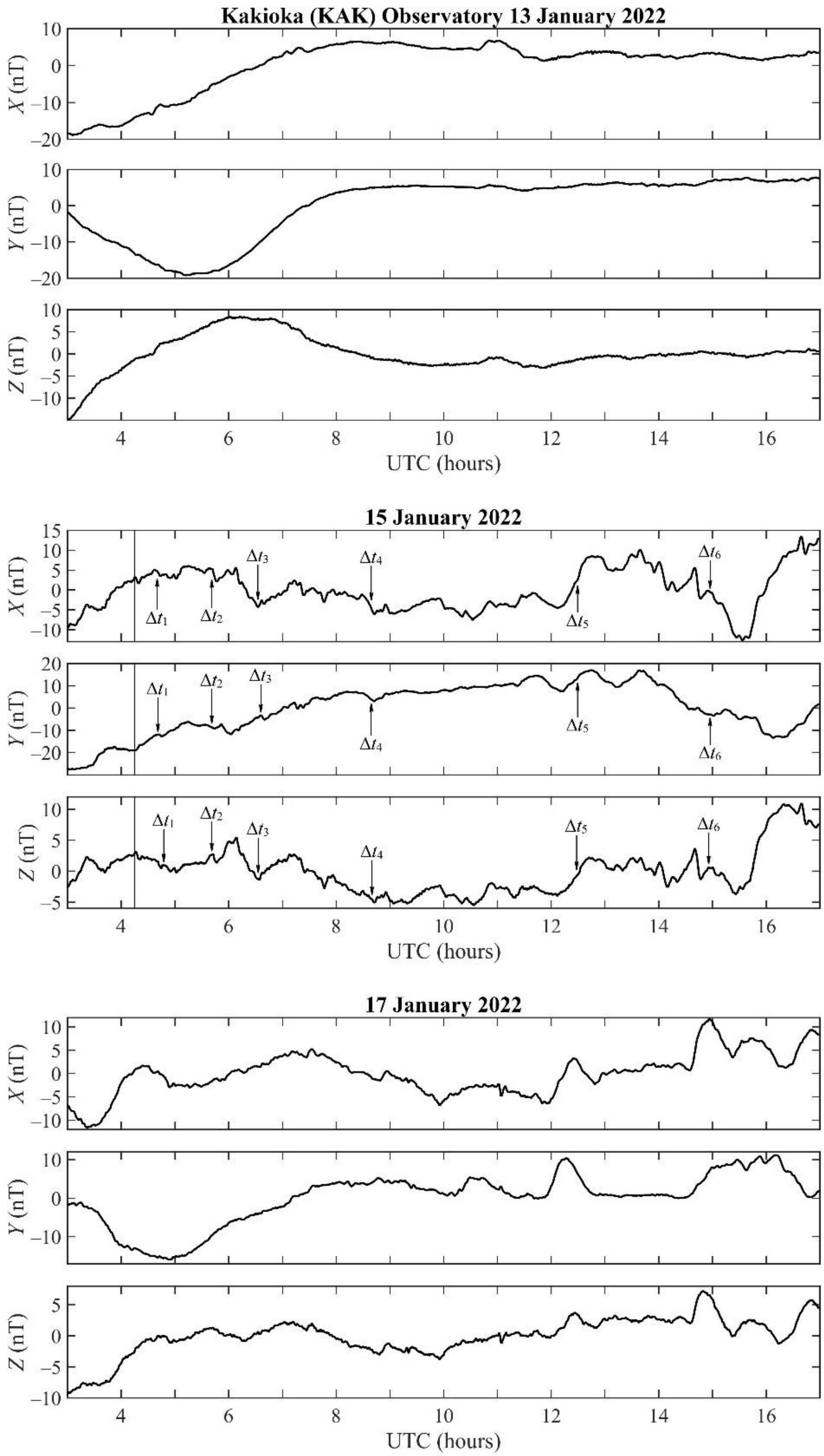


**Figure 14: Same as in Figure 2 but for the KAK Station.**

https://doi.org/10.5194/angeo-2023-27
Preprint. Discussion started: 16 August 2023



*KNY Station.* During 13 January 2022, the trends $\overline{X}$ and $\overline{Z}$ increased from –21 nT to 5 nT from 03:00 UTC to 08:00 UTC (Figure 15), while the trend $\overline{Y}$ was observed to develop a deep drop from 4 nT to –25 nT. From 08:00 UTC to 17:00 UTC, the strength of fluctuations of the geomagnetic field was insignificant, ±1 nT. On 17 January 2022, a deep drop occurred in the $\overline{Y}$ and $\overline{Z}$ trends. The magnitude of fluctuations in all components attained ±5 nT. On 15 January 2022, the magnitudes of the trends in all components increased over the 03:00 UTC to 06:00 UTC period. The strength and time rate of fluctuations also increased. Six groups of perturbation were observed to arrive with time delays of 39 min, 95 min, 140 min, 270 min, 435 min, and 685 min (see Figure 15); the amplitudes of the disturbances attained 4–5 nT. A pronounced *Y*-component oscillation with $T \approx$ 70-min period and an amplitude of 4-nT arrived with the time delay of 435 min.

*MMB Station.* On 13 January 2022, the trend of $X(t)$ increased from –19 nT to 5 nT, and then fluctuated around 2–3 nT (Figure 16). The *Y* component showed a negative bay disturbance, with a strength reduction from –4 nT to –17 nT, which persisted from 03:00 UTC to 08:00 UTC. Then, up to 17:00 UTC, an insignificant rise in this component strength was observed to occur. The *Z*-component, instead, exhibited a positive bay disturbance over the 03:00 UTC to 09:00 UTC period. On 17 January 2022, the strengths of the *X*- and *Y*-components showed variations attaining 10–15 nT, whereas the *Z*-component variations did not exceed 5–6 nT.

On 15 January 2022, the bay reductions by 10 nT, 10 nT, and 3 nT in the strengths of the *X*, *Y*, and *Z* components, respectively, were observed to occur with time delays of 200–225 min and to persist for 210 min to 290 min. In addition, the amplitudes showed quasi-periodic disturbances with amplitudes of a few nanotesla and $T \approx$ 7–20 min.

*SHU Station.* During 13 January 2022, the trend $\overline{X}$ decreased from 3 nT to –2 nT over ~03:30 UTC to 17:00 UTC period (Figure 17), while the trend $\overline{Y}$, instead, increased from –4 nT to 3 nT. The trend $\overline{Z}$ decreased from 4 nT to –2 nT over the 04:00 UTC to 10:00 UTC period and then gradually increased from –2 nT to 1 nT. All components showed fluctuations with amplitudes not exceeding ~1 nT. On 17 January 2022, the trend $\overline{X}$ was first found to fluctuate within the 0–5-nT limits; after 10:00 UTC, some surges and drops attained 10–20 nT, and their durations did not exceed 1 h, whereas the time variations in the *Y*- and *Z*-components showed significant, up to 10–20 nT, fluctuations.

On the day the volcanic explosion occurred, the trend $\overline{X}$ first decreased from 5 nT to –17 nT over the 06:00 UTC to 09:00 UTC period, then it increased from –17 nT to 15 nT. A drop from 15 nT to –15 nT in the $\overline{X}(t)$ dependence was observed to occur from15:00 UTC to 17:00 UTC, while a clearly observed oscillation of the strength with 4-nT amplitude and $T \approx$ 50-min period persisted over the 11:00–13:30 UTC period. The trend $\overline{Y}$ increased from –10 nT to 18 nT over the time interval from 04:00 UTC to 09:40 UTC, next its decrease to –35 nT continued to 15:00 UTC; finally, a ~50 nT surge in the trend persisted for ~1.5 h. The trend $\overline{Z}$ decreased from 20 nT to 0 nT over the 04:00 UTC to 11:00 UTC period. From 11:00 UTC to 16:00 UTC, the $\overline{Z}(t)$ showed a drop from 0 nT to –20 nT, while a clearly observed oscillation with a 6–7-nT amplitude and an ~80-min period lasted from 12:00 UTC to 17:00 UTC.

https://doi.org/10.5194/angeo-2023-27
Preprint. Discussion started: 16 August 2023


Annales Geophysicae
Discussions

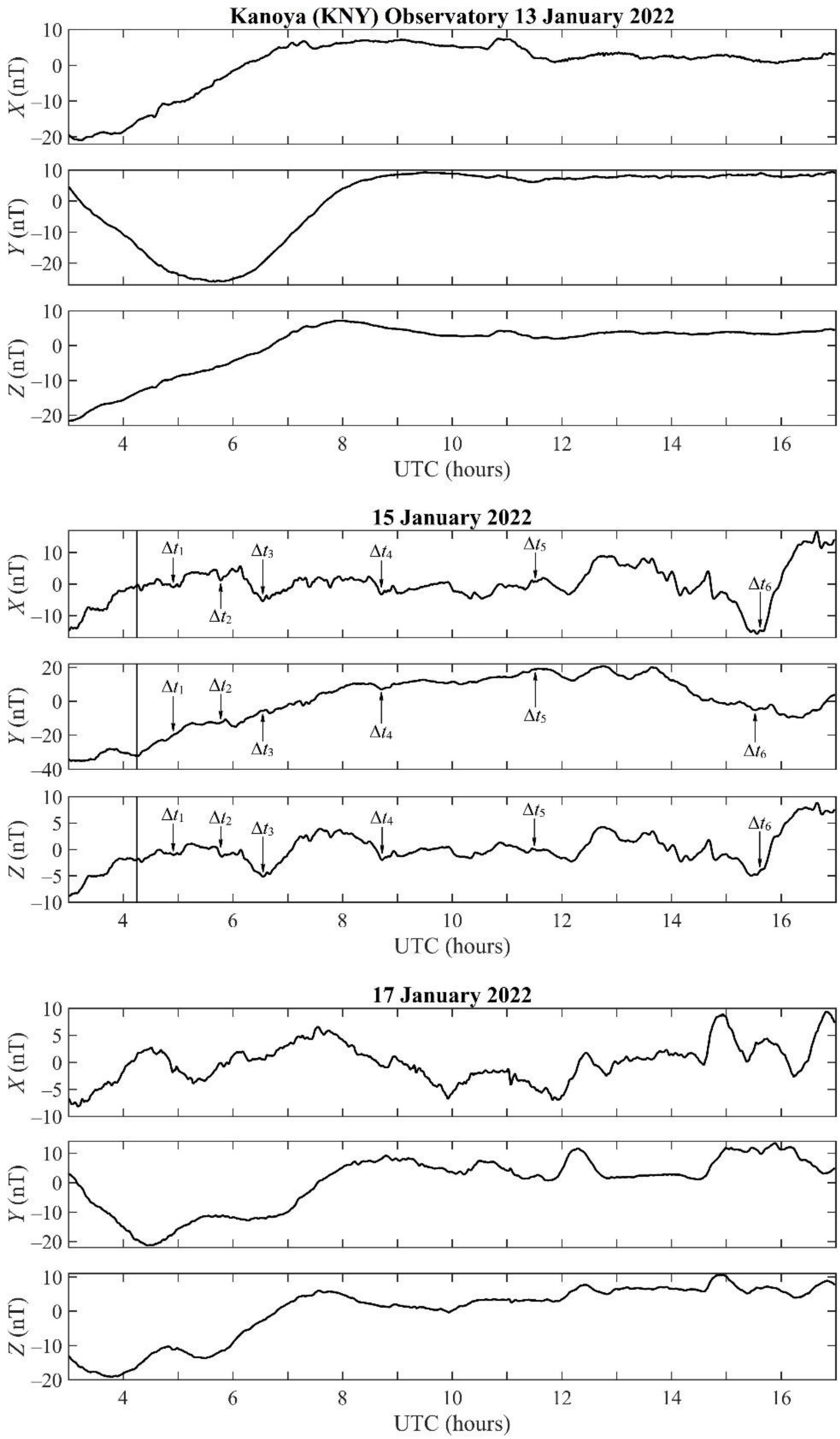


361

362 **Figure 15: Same as in Figure 2 but for the KNY Station.**

https://doi.org/10.5194/angeo-2023-27
Preprint. Discussion started: 16 August 2023


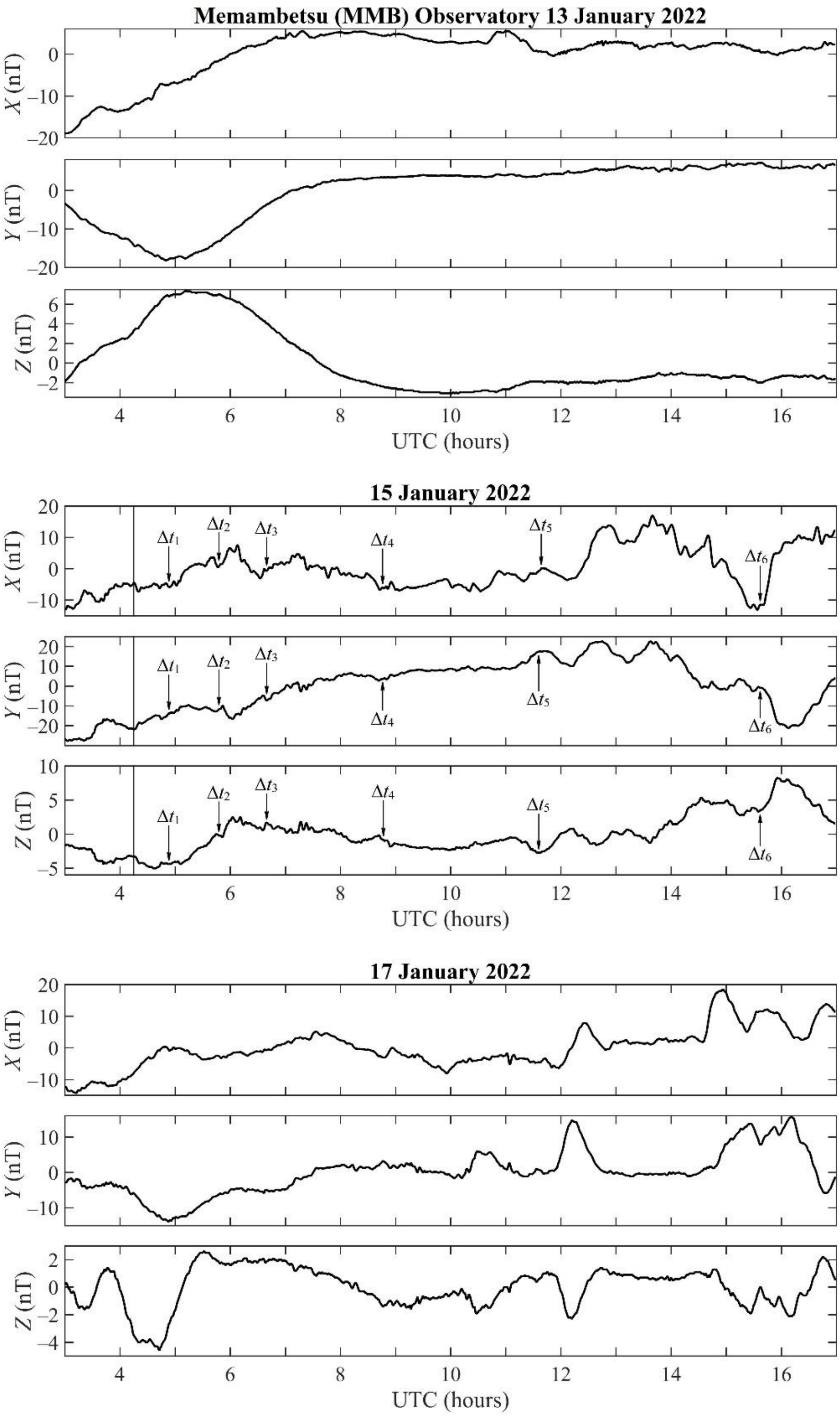


Figure 16: Same as in Figure 2 but for the MMB Station.

https://doi.org/10.5194/angeo-2023-27
Preprint. Discussion started: 16 August 2023


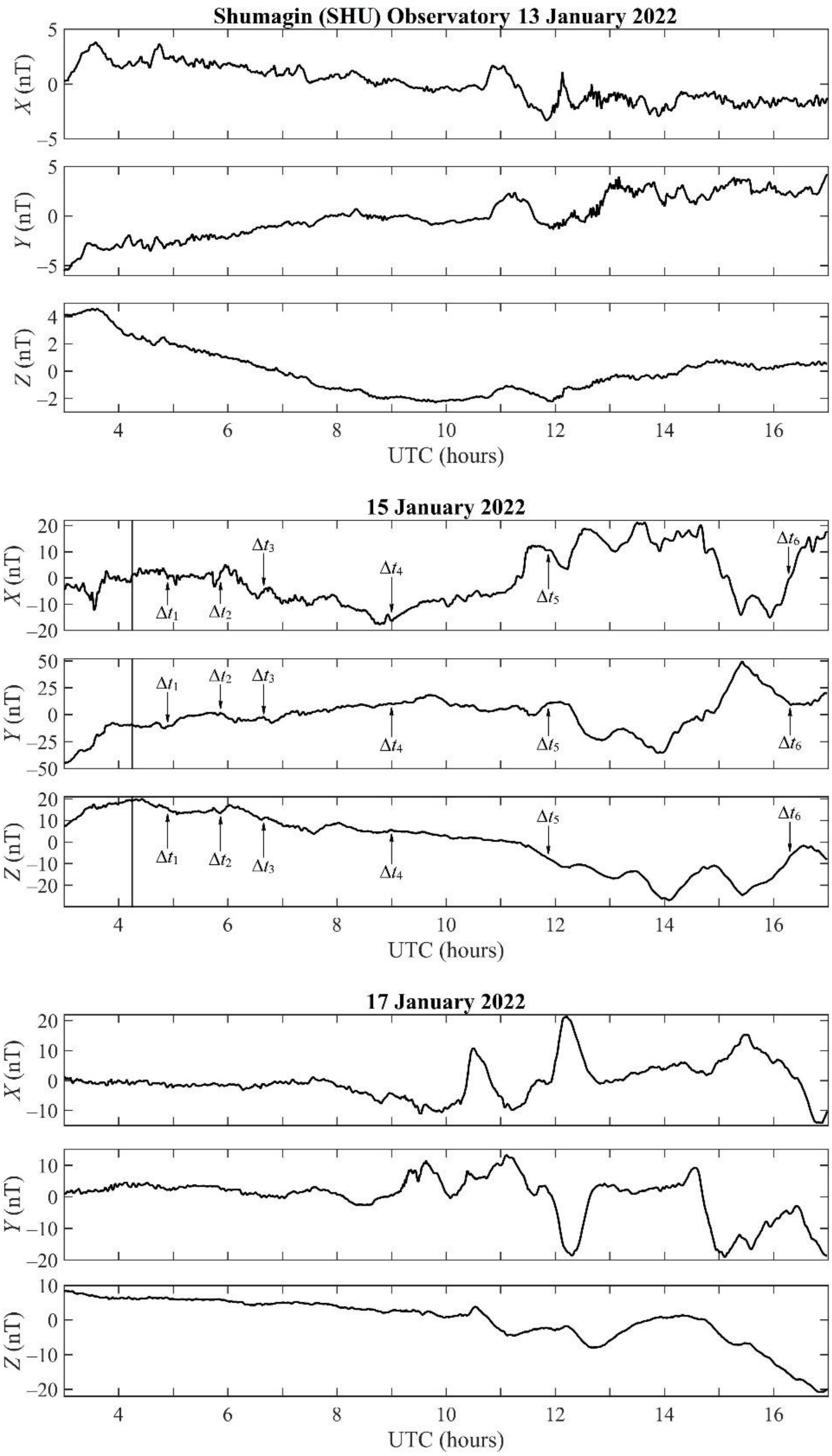


**Figure 17: Same as in Figure 2 but for the SHU Station.**

https://doi.org/10.5194/angeo-2023-27
Preprint. Discussion started: 16 August 2023


*DLT Station.* On 13 January 2022, all components showed insignificant (a few nanotesla) fluctuations in their strengths (Figure 18) over the time period beyond the data gap. 17 January 2022, the trend $\overline{X}$ decreased from 36 nT to –17 nT from 04:00 UTC to 12:00 UTC, then it exhibited fluctuations within the 4–6-nT limits. The trend $\overline{Y}$ decreased from 17 nT to –7 nT after 03:30 UTC. Next its strength showed fluctuations within the ±(2–3)-nT limits. The trend $\overline{Z}$ remained almost constant from 03:00 UTC to 06:00 UTC, then it increased from –25 nT to 10 nT, and after 09:00 UTC it again remained almost constant.

Throughout the day the volcanic explosion occurred, all components showed considerable variations. The trend $\overline{X}$ experienced a bay reduction from ~22 nT to –25 nT over the 06:00–11:00 UTC period. Another drop in the $\overline{X}(t)$ dependence was observed to occur from 13:00 UTC to 17:00 UTC. The $\overline{Y}$ showed significant and long-lasting disturbances from 04:00 UTC to 17:00 UTC. The trend $\overline{Z}$ increased from –9 nT to 4 nT over the 04:20–05:30 UTC period, next a drop in $\overline{Z}$ from 4 nT to 2 nT occurred, which was followed by an increase from 2 nT to 17 nT. After that a steep fall in the trend to 0 nT was first observed, and then a slow decrease from 0 nT to –5 nT. After around 15:30 UTC, the trend once again showed noticeable variations (~5 nT).

*CKI Station.* On 13 January 2022 used as a quiet time reference, the trend $\overline{X}$ showed an insignificant rise to ~26 nT before approximately 05:00 UTC, after which the trend experienced a sharp fall from 26 nT to –10 nT and later was followed by insignificant fluctuations in its magnitude (Figure 19). The trend $\overline{Y}$ first decreased from –3 nT to –13 nT over the 04:00–06:00 UTC period, next, from 06:00 UTC to 10:00 UTC, it experienced a steep rise from –13 nT to 13 nT that was changed by a gradual reduction in the trend to 0 nT at 17:00 UTC. The trend $\overline{Z}$ fell from 5 nT to –3.5 nT over the 03:30 UTC to 06:30 UTC period, whereas it showed two considerable surges, from –2 nT to 2 nT and from –2 nT to 1 nT, over the 09:00–12:00 UTC and 12:00–17:00 UTC periods, respectively. On 17 January 2022, used as a quiet time reference, the trend $\overline{X} \approx 20$ nT from 03:00 UTC to 06:00 UTC. From 06:00 UTC to 10:00 UTC, it was observed to steeply fall from 20 nT to –15 nT. Noticeable surges (by 10 nT to 15 nT) were observed over the 12:00 UTC to 16:00 UTC and 16:00 UTC to 17:00 UTC periods. The trend $\overline{Y}$ sharply increased from –40 nT to 10 nT from 03:00 UTC to 06:00 UTC, and then, fluctuating, gradually decreased from 10 nT to –10 nT at 17:00 UTC. The trend $\overline{Z}$ increased from 0 nT to 15 nT over the 03:00–05:50 UTC period, after this it sharply decreased to –5 nT over a 3-h interval. After 09:00 UTC, the trend $\overline{Z}$ showed fluctuations within the ±(2–3)-nT limits.

https://doi.org/10.5194/angeo-2023-27
Preprint. Discussion started: 16 August 2023


Annales Geophysicae
Discussions

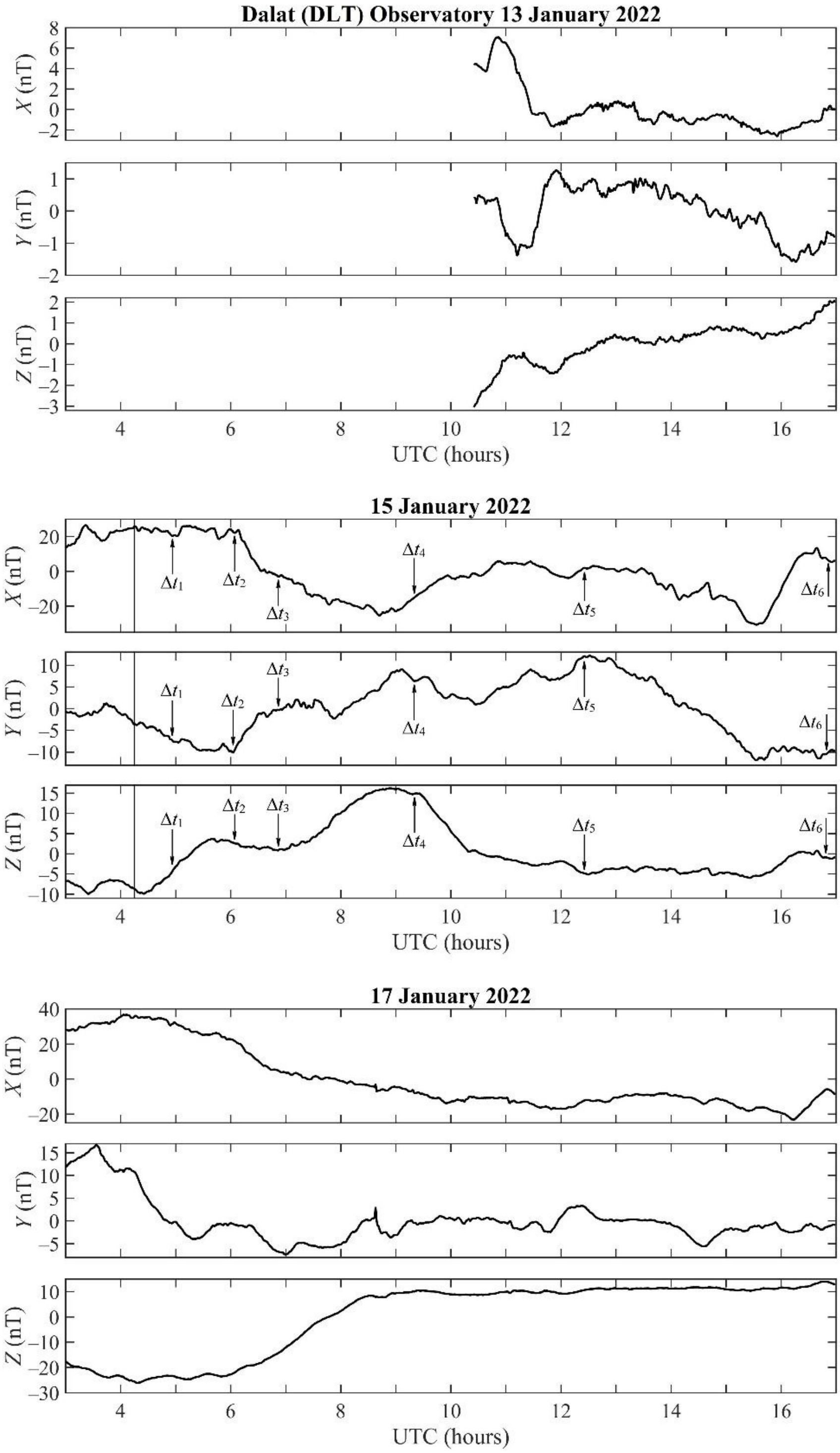


**Figure 18: Same as in Figure 2 but for the DLT station.**

https://doi.org/10.5194/angeo-2023-27
Preprint. Discussion started: 16 August 2023


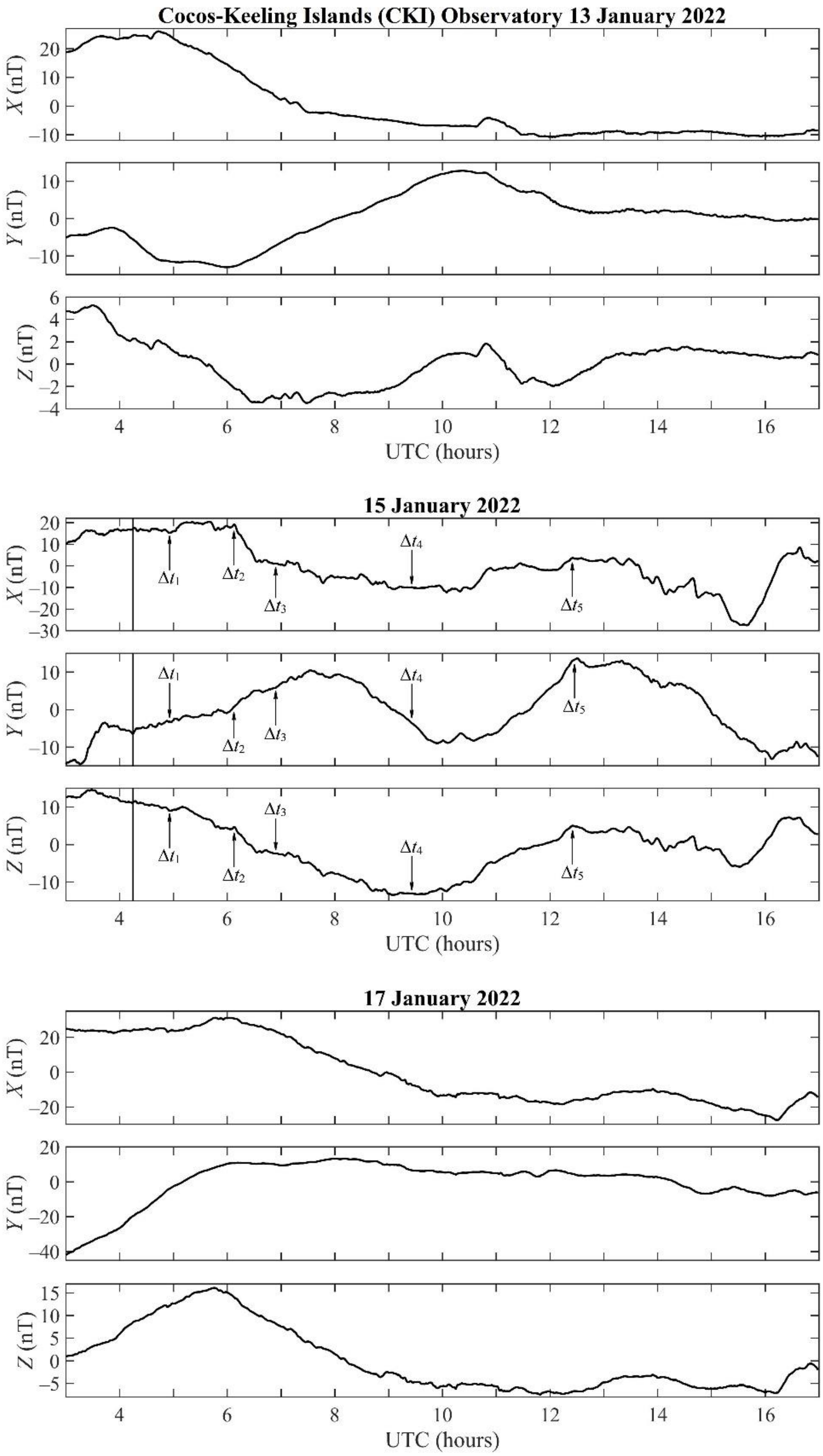


Figure 19: Same as in Figure 2 but for the CKI station.

https://doi.org/10.5194/angeo-2023-27
Preprint. Discussion started: 16 August 2023



On the day the volcanic explosion occurred, all components showed a significant enhancement in their variations. The trend $\overline{X}$ first increased to 05:30 UTC and then sharply decreased from 20 nT to –10 nT after 06:00 UTC. Noticeable increases in $\overline{X}$ from –10 nT to 0 nT occurred during the 10:00–12:00 UTC period. From 13:00 UTC to 17:00 UTC, the trend exhibited a drop from 0 nT to –27 nT. The trend $\overline{Y}$ increased from –5 nT to 10 nT from 04:00 UTC to 07:40 UTC. Next, from 07:40 UTC to 12:30 UTC, $\overline{Y}$ experienced a bay reduction from ~8–10 nT to –8 nT. After 12:30 UTC, the trend $\overline{Y}$ was observed to decrease to –14 nT at 17:00 UTC. The trend $\overline{Z}$ sharply decreased from 15 nT to –13 nT during the 03:30–09:30 UTC period. From 09:30 UTC to 15:00 UTC, the dependence $\overline{Z}(t)$ exhibited a surge from –13 nT to 5 nT. Yet another surge in $\overline{Z}$ to 7 nT was observed to occur from 15:00 UTC to 17:00 UTC.

*GAN Station.* On 13 January 2022, the trend $\overline{X}$ first increased from –12 nT to 21 nT over the 03:00 UTC to 08:00 UTC period, and then decreased from 21 nT to –14 nT during the 08:00–17:00 UTC period (Figure 20). The trend $\overline{Y}$ first increased from –1 nT to 5 nT from 03:00 UTC to 04:00 UTC, then sharply decreased from 5 nT to –25 nT from 04:00 UTC to 08:45 UTC, next increased from –25 nT to 13 nT over the 09:00–12:00 UTC period, and finally gradually decreased from 13 nT to 8 nT at 17:00 UTC. The trend $\overline{Z}$ exhibited two considerable surges, from –4 nT to 5 nT over the 03:00 UTC to 06:00 UTC period, and from –4 nT to 11 nT from 08:30 UTC to 14:00 UTC. On 17 January 2022, the trend $\overline{X}$ first increased from –10 nT to 40 nT from 03:00 UTC to 07:00 UTC, next decreased to –20 nT at 12:00 UTC, and then exhibited fluctuations within the ±5-nT limits. The trend $\overline{Y}$ showed short-term (~1–2 h) increases by up to 4–5 nT, in addition to a powerful surge (from –20 nT to 26 nT) during the 03:00–11:30 UTC period. The trend $\overline{Z}$ exhibited a powerful surge from –3 nT to 27 nT from 03:00 UTC to 10:00 UTC; relatively small undulations of up to 5–6 nT were observed to occur after 10:00 UTC.

On the day the volcanic explosion occurred, all components exhibited noticeably enhanced variability. The trend $\overline{X}$ first increased from –7 nT to 28 nT over the 03:00 UTC to 06:00 UTC period and then reduced from 28 nT to –3 nT from 06:00 UTC to 10:30 UTC; in addition to variations within the ±5-nT limits, a drop from 5 nT to –28 nT was observed to occur over the 13:00–16:30 UTC period. The trend $\overline{Y}$ also first increased from –20 nT to 7 nT over the 03:00–06:30 UTC period, and then a deep drop occurred from 7–18 nT to –8 nT over the 06:30 UTC to 14:25 UTC period. Over the 14:25–17:00 UTC period, the trend $\overline{Y}$ decreased from 18 nT to 2 nT. The trend $\overline{Z}$ first increased to 22 nT before 06:00 UTC. Next, a deep drop (from 22 nT to –20 nT) followed over approximately 7 h. And finally, the moderate (up to 10–15 nT) variations in $\overline{Z}$ were observed to occur. It should be noted that synchronous geomagnetic bay disturbances were observed to occur uncertainly at this most distant recording station.

https://doi.org/10.5194/angeo-2023-27
Preprint. Discussion started: 16 August 2023


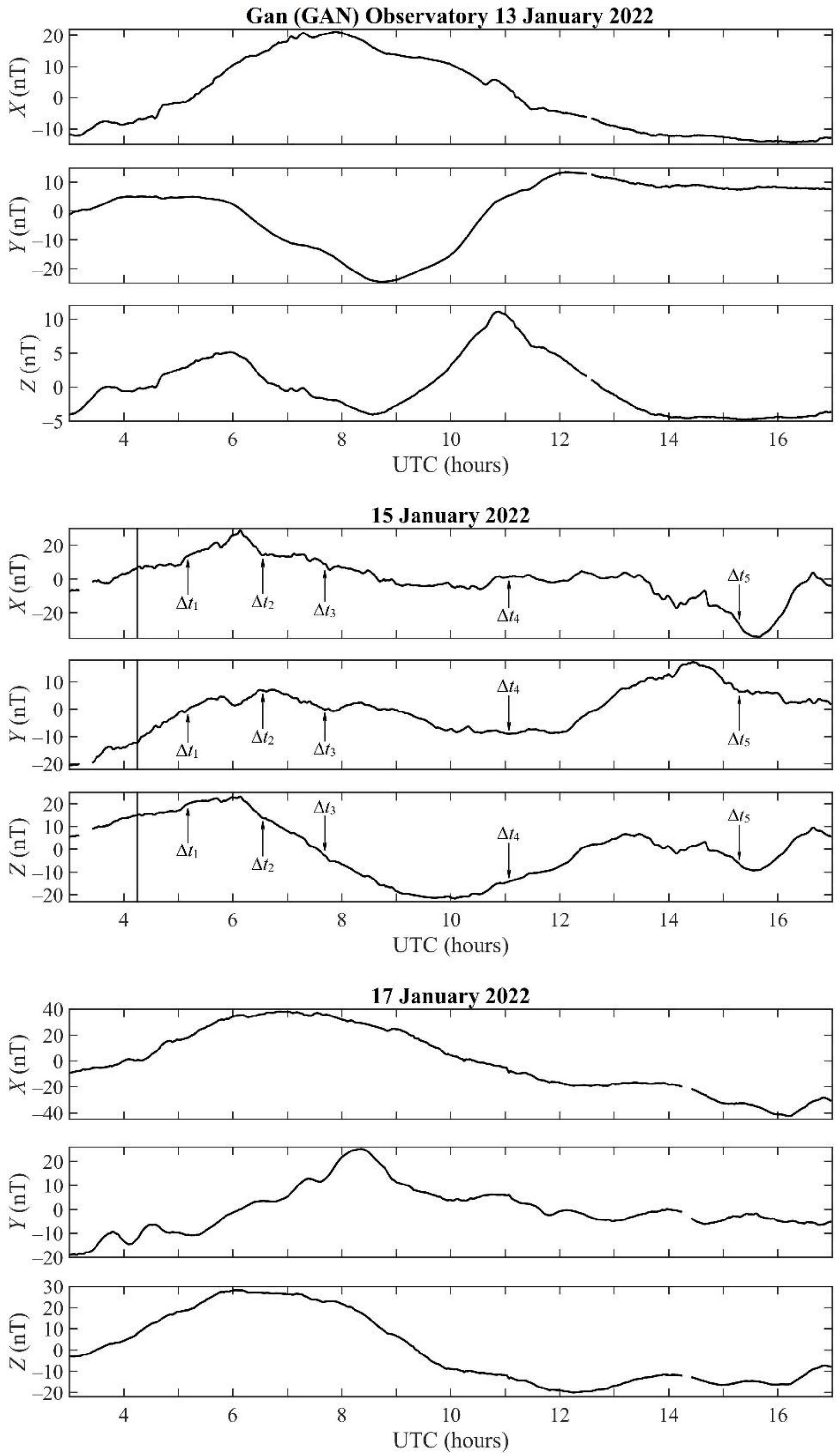


**Figure 20: Same as in Figure 2 but for the GAN station.**

https://doi.org/10.5194/angeo-2023-27
Preprint. Discussion started: 16 August 2023



## 7 Statistical data analysis of the bay excursions in geomagnetic field strengths

Table 4 shows the basic parameters of the bay disturbances of the geomagnetic field, viz., the magnitudes ΔX, Δ*Y*, Δ*Z*, the time delays τ, and the durations Δ*T* of the northward component, *X*, of the eastward component, *Y*, and of the vertical component, *Z*, at nineteen stations. As can be seen from Table 4, the values of Δ*X*, Δ*Y*, and Δ*Z* were most often negative except for the data from the API and PPT stations, which were located at a distance, *r*, of 840 km and 2,730 km, respectively, away from the volcano. The time delay showed a tendency to increase with increasing distance from the volcano, and the duration of disturbances exhibited the same tendency as the time delay. Table 4 shows that the strength of disturbances exhibits a tendency to decrease with increasing *r*.

Table 4. Basic parameters of bay disturbances in the geomagnetic field.

| Station | $\Delta X$ (nT) | $\tau_X$ (min) | $\Delta T_X$ (min) | $\Delta Y$ (nT) | $\tau_Y$ (min) | $\Delta T_Y$ (min) | $\Delta Z$ (nT) | $\tau_Z$ (min) | $\Delta T_Z$ (min) |
|---|---|---|---|---|---|---|---|---|---|
| API | 15 | 16 | 90 | 28 | 16 | 146 | –13 | 16 | 130 |
| PPT | 8 | 45 | 90 | 8 | 45 | 100 | | | |
| EYR | –40 | 50 | 120 | –25 | 50 | 120 | –15 | 50 | 120 |
| CNB | –20 | 100 | 120 | –50 | 60 | 178 | –15 | 60 | 120 |
| CTA | –18 | 105 | 130 | –63 | 60 | 150 | –30 | 60 | 150 |
| MCQ | –80 | 100 | 180 | –50 | 100 | 150 | –30 | 80 | 150 |
| HON | –10 | 75 | 180 | –5 | 75 | 180 | –2 | 75 | 180 |
| ASP | –15 | 100 | 230 | –50 | 75 | 240 | –15 | 75 | 240 |
| KDU | –10 | 110 | 210 | –30 | 110 | 210 | –15 | 110 | 200 |
| IPM | –10 | 110 | 220 | –8 | 110 | 220 | –2 | 100 | 220 |
| GNG | –15 | 120 | 270 | –50 | 120 | 270 | –30 | 120 | 270 |
| LRM | –10 | 140 | 270 | –10 | 140 | 265 | –5 | 140 | 265 |
| KAK | –10 | 180 | 270 | –8 | 165 | 260 | –8 | 165 | 300 |
| KNY | –10 | 115 | 270 | | | | –8 | 120 | 270 |
| MMB | –10 | 165 | 240 | –8 | 165 | 240 | –8 | 165 | 240 |
| SHU | –10 | 105 | 220 | –10 | 150 | 200 | –10 | 150 | 200 |
| DLT | –20 | 165 | 240 | –8 | 165 | 240 | | | |
| CKI | –12 | 170 | 240 | –15 | 175 | 250 | –10 | 165 | 240 |
| GAN | –10 | 240 | 240 | –8 | 240 | 240 | –15 | 240 | 240 |

https://doi.org/10.5194/angeo-2023-27
Preprint. Discussion started: 16 August 2023

Annales Geophysicae Discussions

Figure 21 presents scatter plots of time delay versus distance from the volcano, which reveal the following linear dependences:

$$\tau_X = 17.17r + 9.3,\ \sigma \approx 22.1\ \text{min},\ R^2 \approx 0.83, \quad (1)$$

$$\tau_Y = 19.93r - 10,\ \sigma \approx 12\ \text{min},\ R^2 \approx 0.96, \quad (2)$$

$$\tau_Z = 19.63r - 12,\ \sigma \approx 14.1\ \text{min},\ R^2 \approx 0.94, \quad (3)$$

where distance is in Mm, time delay is in min, σ is a root mean square error, $R^2$ is an adjusted coefficient of determination.

The individual points are fit with the following straight lines (Figure 22):

$$\Delta T_X = 18.44r + 86.5,\ \sigma \approx 36.3\ \text{min},\ R^2 \approx 0.68, \quad (4)$$

$$\Delta T_Y = 14.29r + 115.6,\ \sigma \approx 34.5\ \text{min},\ R^2 \approx 0.60, \quad (5)$$

$$\Delta T_Z = 15.63r + 109.8,\ \sigma \approx 39.5\ \text{min},\ R^2 \approx 0.56. \quad (6)$$

The relations (1) – (3) and (4) – (6) indicate that the time delay and the duration of disturbance indeed increase with distance from the volcano. The formation of disturbance is close to root mean square deviations in time delays, i.e., to 12–22 min.

https://doi.org/10.5194/angeo-2023-27
Preprint. Discussion started: 16 August 2023

Annales Geophysicae
Discussions
Open Access
EGU

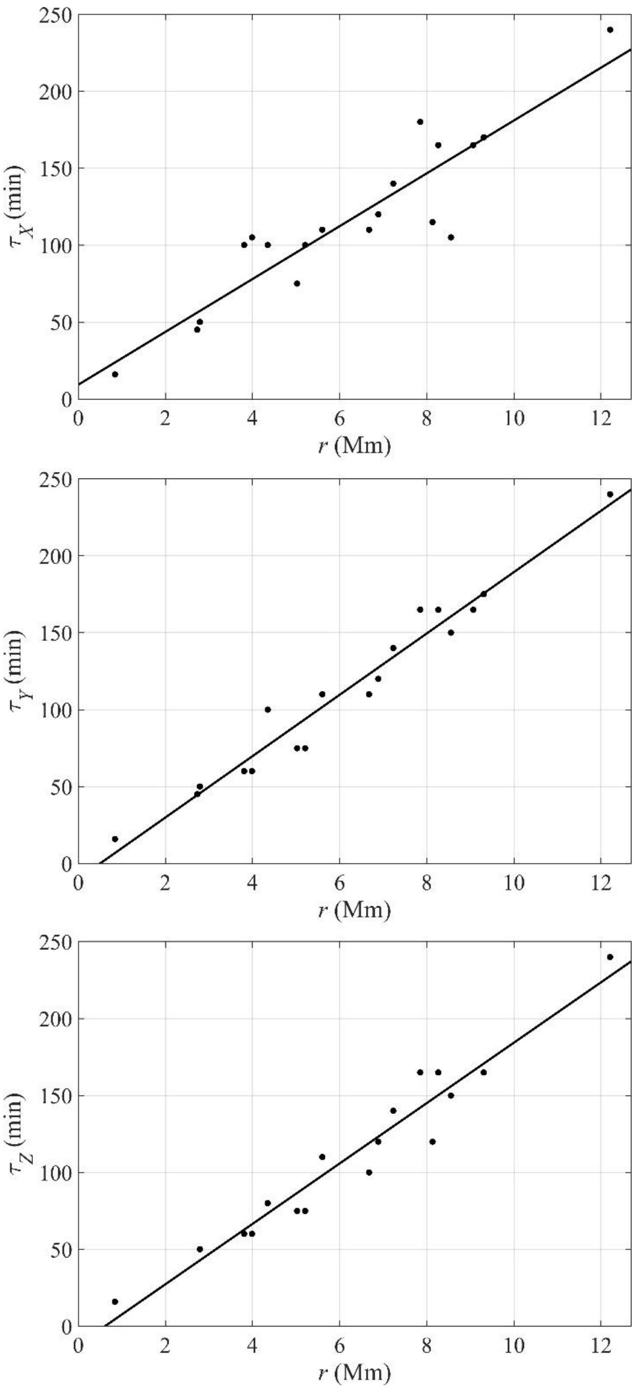


**Figure 21: Time delay of bay disturbance in the geomagnetic field vs distance, *r*, from the volcano and the estimated regression line superimposed on the scatter plot.**

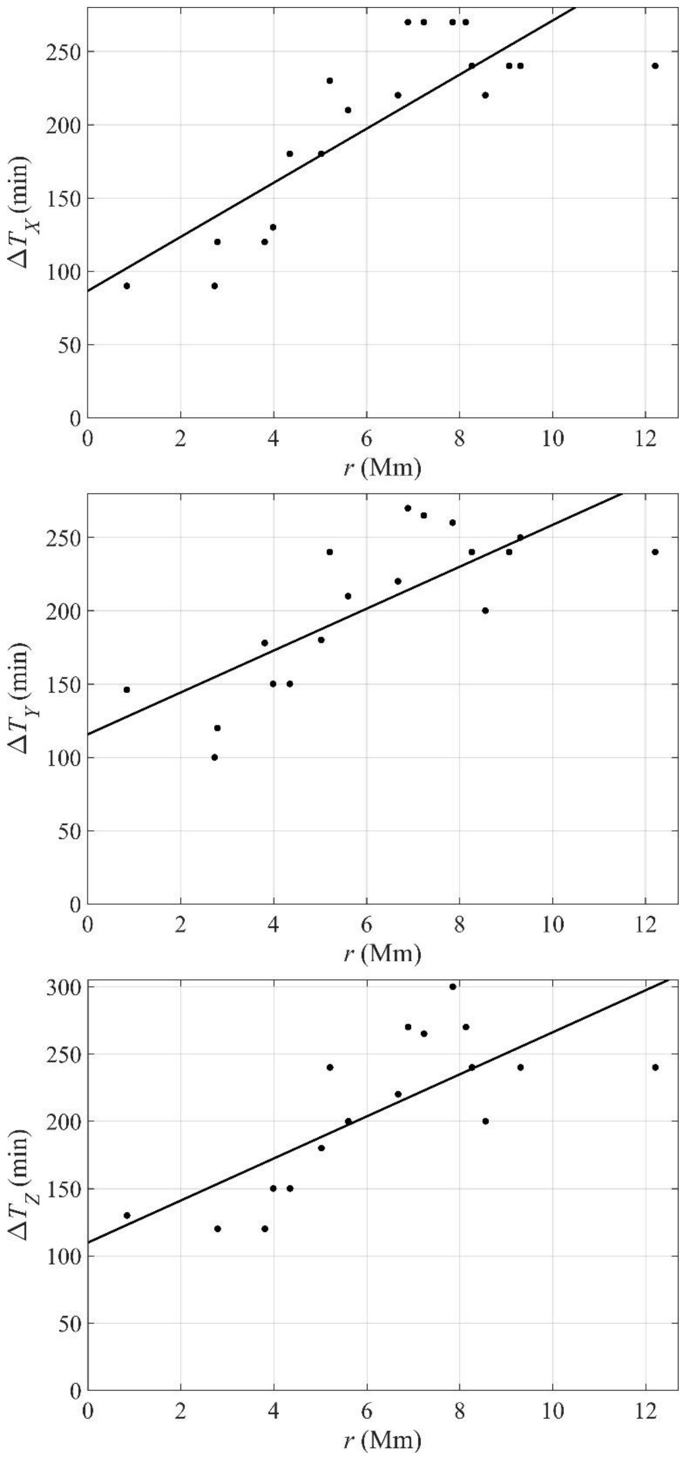


**Figure 22: Duration of bay disturbance in the geomagnetic field vs distance from the volcano and the estimated regression line superimposed on the scatter plot.**

https://doi.org/10.5194/angeo-2023-27
Preprint. Discussion started: 16 August 2023

Annales Geophysicae Discussions Open Access EGU

Histograms showing the distributions of all $\Delta X$, $\Delta Y$, and $\Delta Z$ are presented in Figure 23. The most probable values of these disturbances are seen to be as follows: for the northward component $\Delta X = -(9.0 \pm 5.1)$ nT, for the eastward component $\Delta Y = -(10.5 \pm 5.6)$, and for the vertical component $\Delta Z = -(6.3 \pm 3.1)$ nT, and $-(25.0 \pm 5.0)$ nT.

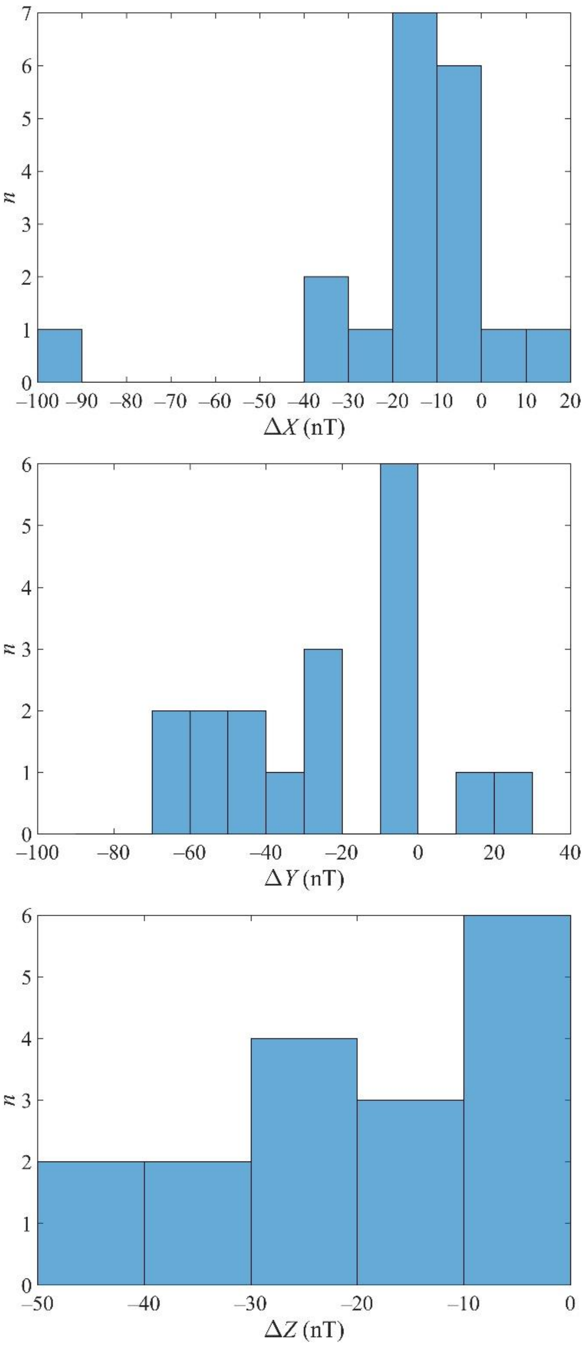


**Figure 23: Histogram showing the distribution of excursions in bay disturbances in the geomagnetic field.**

https://doi.org/10.5194/angeo-2023-27
Preprint. Discussion started: 16 August 2023

Annales Geophysicae Discussions
Open Access
EGU

## 8 Statistical data analysis of the quasi-periodic variations in geomagnetic field magnitudes

The time delays of a possible response of the magnetic field to the volcanic explosion and the apparent speeds for six groups of characteristic variations in the components of the geomagnetic field are presented in Table 3, which show that the variations in the eastward component *Y* are seen most clearly. Figure 24 presents a scatter plot of time delay versus distance from the volcano for all the data presented in Table 3, which reveal the following linear dependences:

$$\Delta t_1 = 4.157r + 5.1, \quad \sigma = 0.32 \text{ min}, \quad R^2 = 0.9995, \tag{7}$$

$$\Delta t_2 = 11.14r + 4.6, \quad \sigma = 0.55 \text{ min}, \quad R^2 = 0.9998, \tag{8}$$

$$\Delta t_3 = 16.66r + 4.6, \quad \sigma = 0.47 \text{ min}, \quad R^2 = 0.9999, \tag{9}$$

$$\Delta t_4 = 33.13r + 4.6, \quad \sigma = 1.60 \text{ min}, \quad R^2 = 0.9998, \tag{10}$$

$$\Delta t_5 = 53.11r + 6.1, \quad \sigma = 9.98 \text{ min}, \quad R^2 = 0.9969, \tag{11}$$

$$\Delta t_6 = 82.97r + 7.7, \quad \sigma = 2.61 \text{ min}, \quad R^2 = 0.9999. \tag{12}$$

If $r \to 0$, then $\Delta t_0 \approx 4.6$–$7.7$ min. Such a time interval is needed for the wave to reach ionospheric heights, or more precisely, *E* region dynamo heights.

Use of relations in Eqs. (7) – (12) and the formula given by

$$v = \left( \frac{d\Delta t}{dr} \right)^{-1}$$

yields the following average speeds: $v_1 \approx 4$ km/s, $v_2 \approx 1.5$ km/s, $v_3 \approx 1$ km/s, $v_4 \approx 503$ m/s, $v_5 \approx 314$ m/s, and $v_6 \approx 209$ m/s. These values are close to the values inferred from the histograms in Figure 25.

The horizontal apparent speed of propagation of disturbances can be estimated from the following relation:

$$v = \frac{r}{\Delta t - \Delta t_0}$$

where $\Delta t_0$ is the time taken for the blast wave to travel from the volcano to the *E* region dynamo.

https://doi.org/10.5194/angeo-2023-27
Preprint. Discussion started: 16 August 2023


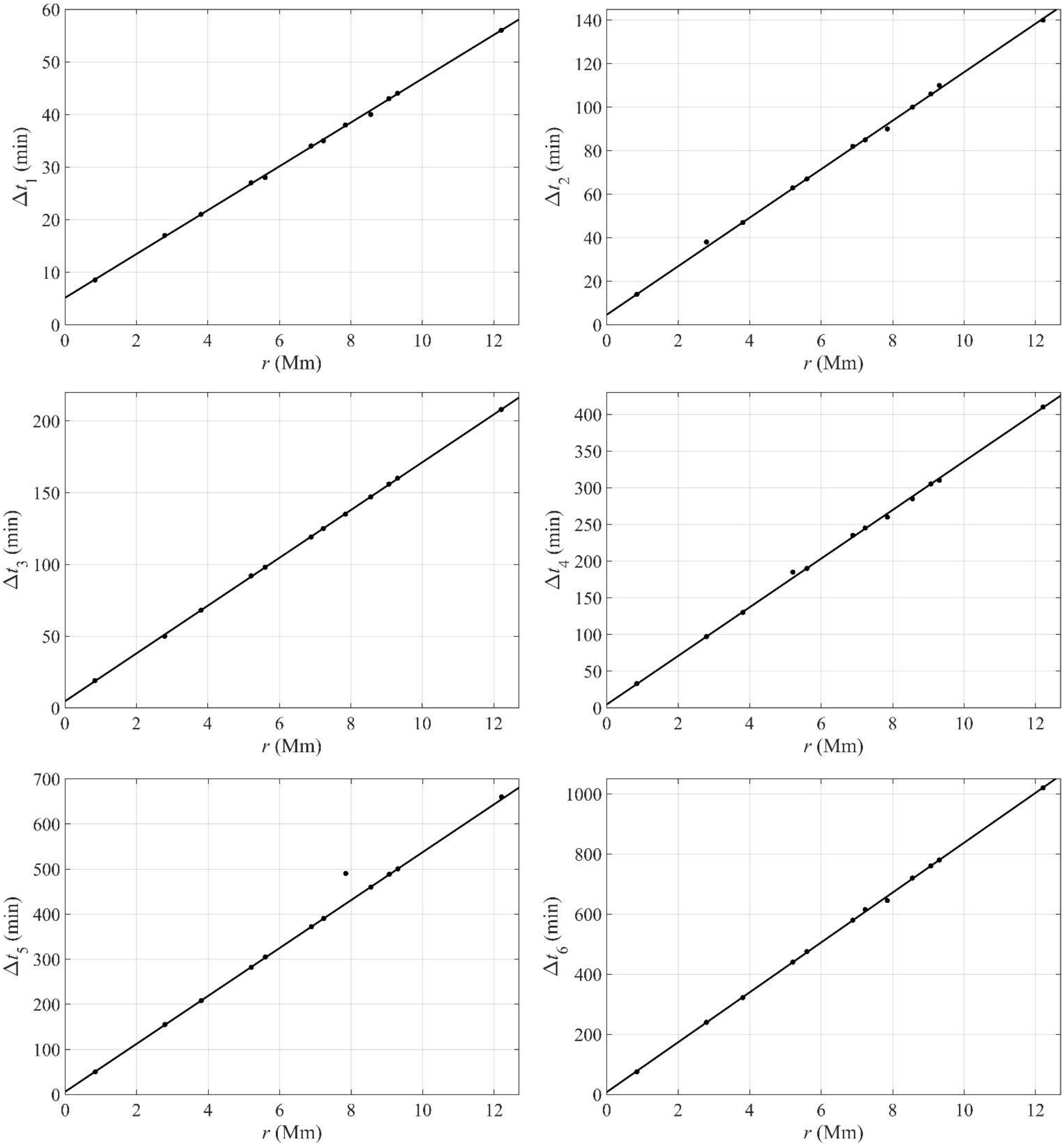


**Figure 24: Time delay of the onset of quasi-periodic disturbances in the geomagnetic field vs distance from the volcano and the estimated regression line superimposed on the scatter plot.**

https://doi.org/10.5194/angeo-2023-27
Preprint. Discussion started: 16 August 2023

Annales Geophysicae
Discussions

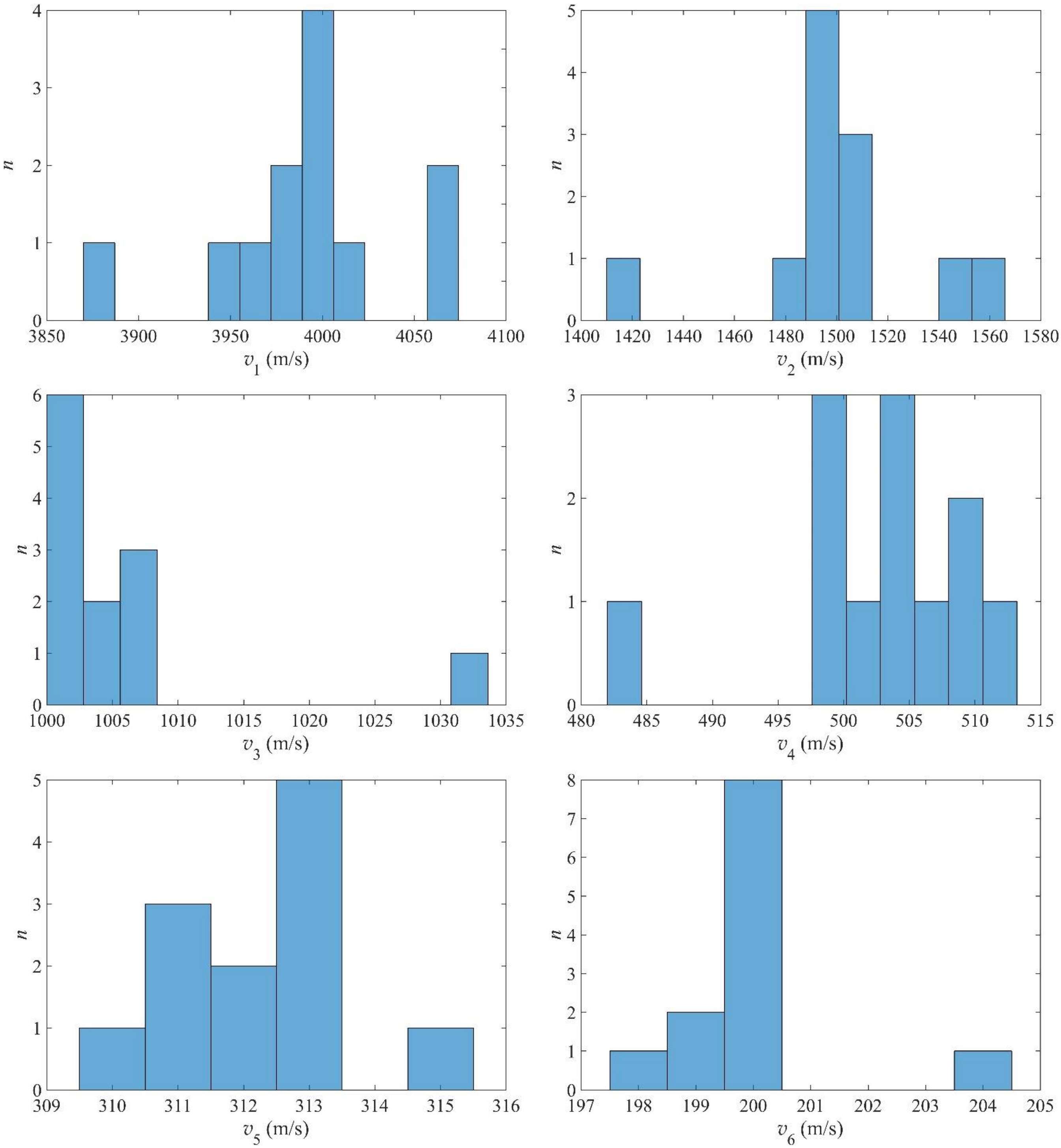


**Figure 25: Histogram showing the distribution of the apparent speeds of propagation of quasi-periodic disturbances in the geomagnetic field.**

https://doi.org/10.5194/angeo-2023-27
Preprint. Discussion started: 16 August 2023

Annales Geophysicae Discussions

## 9. Discussion

*Bay disturbances of the geomagnetic field*. During the day the Tonga volcanic explosion occurred, all three components usually exhibited geomagnetic bay disturbances whose absolute values were observed to be 10–60 nT, and the disturbances themselves were more often seen to be negative. The eastward component $Y$ experienced the largest disturbances, with the average value of –53 nT, whereas disturbances in the $X$ and $Z$ components were observed to be, on average, –15 nT. The smallest disturbance took place at the PPT station. The geomagnetic bay disturbances were virtually absent, or, more precisely, did not exceed –(2–8) nT also at the IPM station, which was located east of the volcano as well. This can be explained by the location of these stations on the night side of the Earth where the electron and electric current densities were approximately an order of magnitude smaller than in the sunlit ionosphere.

Disturbances were insignificant and unclear at the GAN station, the most distant station included in this study.

It should be stressed that the bay variations in the magnitudes of all geomagnetic field components did not exceed 5–10 nT during the days used as a quiet time reference. This observation supports the idea that the geomagnetic bay disturbances observed on 15 January 2022 were due to the volcanic explosion. However, this is a necessary but not sufficient condition for the volcanic explosion to be the cause of the effect.

A sufficient condition is a tendency for the time delay and duration of bay disturbance to grow with distance from the volcano, while a tendency for the disturbance strength was to decrease with distance from the volcano (see Figures 21 and 22).

The relations in Eqs. (1) – (3) suggest that, in the limit $r \to 0$, the minimum in the time delay, $\tau_{\min}$, is determined by root mean square error in the approximation, which is close to 14–22 min for the $X$, $Y$, and $Z$ components. The disturbance from the volcano takes such a time interval to travel from the volcano to the $E$ region dynamo, $z \approx 90$–150 km altitude, and to generated magnetic disturbance. The relations in Eqs. (1) – (3) permit estimates of the average speeds of the disturbances to be made using the relation given by

$$v = \left(\frac{d\tau}{dr}\right)^{-1}.$$

Then, $v_X \approx 970 \pm 235$ m/s, $v_Y \approx 836 \pm 103$ m/s and $v_Z \approx 849 \pm 121$ m/s. These magnitudes of the speeds are close to the blast wave speed [Chernogor, 2023b; Chernogor, 2023c].

It is important that the magnitudes of the speeds obtained are close to the speed of propagation of the disturbances in the electron density, $N$, and in the total electron content [Chernogor, 2023a]. This means that the formation of the ionospheric hole is the cause of the bay excursions in the geomagnetic field [Chernogor, 2023a].

Estimation of the magnitude of a bay disturbance in the geomagnetic field may be performed from the average daytime value of $N$ in the $E$ region dynamo of $(2–3) \times 10^{11}$ m$^{-3}$ and a neutral wind speed of $w \approx 100$ m/s. Then, the electric current density in the ionosphere is given by

$j_0 = eNw \approx (3.2\text{–}4.8) \times 10^{-6}$ A/m$^2$

where $e$ is the charge of an electron. The disturbance in $N$ within the ionospheric hole is estimated to be 5–20%, which yields the perturbation in the ionospheric current of $\Delta j \approx (1.6\text{–}9.6) \times 10^{-7}$ A/m$^2$. The estimate of the disturbance in the magnetic field follows from Maxwell's curl equation, given by

$$\Delta B \approx \mu_0 \Delta j \Delta z \qquad (13)$$

where $\mu_0$ is magnetic permeability, $\Delta z \approx 50$ km is the thickness of the dynamo region. Substituting the numerical magnitudes yields $\Delta B \approx 10\text{–}60$ nT, which is in excellent agreement with observations (~10–60 nT).

Thus, there is every reason to believe that the bay disturbances of the components of the geomagnetic field are related to the generation of the ionospheric hole as a result of the explosion of Tonga volcano.

*The effect of atmospheric acoustic resonance*. The station nearest to Tonga volcano is the API Station. The $Y$ component exhibited the first perturbation over the 04:21–04:57 UTC period, i.e., the time delay was observed to be $\Delta t_0 \approx 6$ min. The acoustic wave take such a time interval to travel to the ionospheric $E$ region where dynamo electric fields are generated and where the generation of this magnetic effect occur. The sound wave is reflected at an altitude of $z_r \approx \overline{v}_x \Delta t_0 \approx$ 110–120 km (where $\overline{v}_x \approx 300\text{–}330$ m/s is an average speed of sound), i.e., in the $E$ region dynamo. It is important that the period of the disturbance $T_0 \approx 4\text{–}4.5$ min and its duration $\Delta T_0 \approx 32\text{–}36$ min. These values indicate that the magnetic effect have been generated by the atmospheric acoustic resonance in the Earth–$E$ region dynamo cavity, where the volcanic explosion excited the vibrations.

Since the API station is located at a range of ~840 km from the volcano, the radius, $r_L$, of the footprint of the magnetic flux tube associated with the volcano is equal or greater than 1,000 km. This means that the magnetic effect from the atmospheric acoustic resonance could be observed in the magnetically conjugate region. Indeed, oscillations with the same period, $T_0$, duration $\Delta T_0$, and ~0.2-nT amplitude, were observed by [Iyemori et al., 2022; Yamazaki et al., 2022]. It is important that the time delay was equal to $\Delta t_0 \approx 6$ min. This means that the disturbance from the API station was transferred to the HON station along the magnetic flux tube ~10 Mm long at an Alfvén speed, $v_A$, of ~1 Mm/s for ~10 s, which much shorter than $\Delta t_0$. It should be noted that the HON station is located about 900 km from the center of the magnetic flux tube, and $r_L > 900$ km.

*Quasi-periodic disturbances*. Other disturbances with other time delays were superimposed on the disturbance due to acoustic resonance (see Table 3). In total, the number of such disturbances could be six. Table 3 shows that six groups of disturbances in the geomagnetic field also took place at other stations. It is important that the time delay increases with distance from the volcano. The premise of requiring the time delays of the magnetic disturbances due to the volcanic explosions to explain our observations is clearly supported by the INTERMAGNET Magnetometer Observatory data.

The values of the speeds were close to 4 km/s, 1.5 km/s, 1 km/s and 500 m/s, 313 m/s, and 200 m/s. All these speeds have physical significance. The first and second group of speeds correspond to the speeds of the fast and slow MHD waves [Sorokin and Fedorovich, 1982]. Approximately the same speeds were observed during powerful rocket launches [Chernogor, 2009; Chernogor and Blaunstein, 2013]. The speed of $v_3 \approx 1$ km/s is characteristic of blast waves. This speed was revealed after the Tonga volcanic explosion by [Matoza et al., 2022a; Matoza et al., 2022b]. The speed $v_4$ pertains to atmospheric gravity waves at ionospheric heights [Chen et al., 2022; Themens et al., 2022]. Lamb waves that are generated by massive releases of energy (exceeding 10 Mt of TNT) propagate at a speed of $v_5 \approx 313$ m/s over the Earth's surface virtually without damping and partially penetrate to ionospheric heights along their propagation paths [Chernogor, 2022a; Chernogor, 2022e; Chernogor, 2023a; Kubota et al., 2022; Lin et al., 2022; Zhang et al., 2022a]. The smallest speed of $v_6 \approx$ 200 m/s probably pertains to an average speed of tsunami, which was observed after the volcanic eruption and generated ionospheric disturbances [Carvajal et al., 2022; Ramírez-Herrera et al., 2022; Tanioka et al., 2022; Terry et al., 2022].

*Estimation of the quasi-periodic effects.*

The amplitude of quasi-periodic disturbances usually showed variations not exceeding 1–3 nT. Such disturbances were generated by quasi-periodic disturbances arising in the electric current density at *E* region dynamo heights from the action of waves launched by the volcanic explosion.

The difference, $w_m$, in the drift velocities of ions and electrons, which are driven by the drag force of the neutral atmosphere, causes the dynamo current density given by the relation

$$j = eNw_m.$$

The integrated in altitude current density is given by

$$J = \int_{\Delta z} j(z)dz.$$

Then, the amplitude of the quasi-periodic disturbance in the geomagnetic field is given by the following expression:

$$\Delta B_a \approx \mu_0 J.$$

If $N \approx (2–3) \times 10^{11}$ m$^{-3}$ on the sunlit side of the Earth, and $w_m \approx 0.3–1.5$ m/s, then $j \approx (1–7.2) \times 10^{-8}$ A/m$^2$, $J \approx (4.8–36) \times 10^{-4}$ A/m, and $\Delta B_a \approx 0.6–4.5$ nT. These estimates are seen to be close to magnitudes observed (~1–3 nT).

Thus, the disturbances in the geomagnetic field described above were observed on 15 January 2022 and were absent during the days used as a quiet time reference. Consequently, they were most probably due to the volcanic eruption. These disturbances were transported by the waves of various physical nature, viz., the fast and slow MHD waves, blast waves, atmospheric gravity waves, Lamb waves, and ionospheric waves that arises from the tsunami.

## 8 Conclusions

Analysis of the data acquired at nineteen INTERMAGNET magnetic observatories revealed the following.

(1) During the day of the Tonga volcanic explosion, the variations in the magnitude of all components of the geomagnetic field varied less monotonically than during the days used as a quiet time reference. The strength of fluctuations also enhanced. All these factors indicated that the volcanic explosion led to the registered magnetic effect.

(2) The geomagnetic bay disturbances in all components of the geomagnetic field were observed to occur with a time delay increasing with distance from the volcano from a few tens of minutes to 100–200 min. The magnitude of the effect changed from ~10 nT to ~60 nT. The eastward component (*Y*) exhibited the greatest variations. The time delay and duration of the disturbances increased with distance from the volcano, but amplitudes of the disturbances, instead, decreased. The speed of propagation of the bay disturbances was close to the speed of the blast waves, approximately 700–1,000 m/s. Geomagnetic bay disturbances were weakly expressed or were virtually absent on the night side of the planet. The premise that the geomagnetic bay disturbances are closely related to the volcanic blast wave-induced formation of the ionospheric hole has been validated.

(3) The quasi-periodic disturbances in the geomagnetic field arrived at the magnetic observatories with different time delays. Six main groups of disturbances were identified. It is important that the time delay increases with distance from the volcano in each group. The apparent speeds of propagation of the disturbances in each group have been estimated, and the values of these speeds are as follows: 4 km/s, 1.5 km/s, 1 km/s and 500 m/s, 313 m/s, and 200 m/s. The first two speeds pertain to the fast and slow MHD waves, the third to the blast wave, the fourth to the atmospheric gravity wave, the fifth to the Lamb wave, and the six speed pertain to the tsunami.

(4) The magnetic effect due to the atmospheric acoustic resonance in the Earth – *E* region dynamo cavity where vibrations were excited by the volcanic explosion was observed at API Station, the nearest to Tonga volcano. The period of the disturbance was estimated to be $T_0 \approx$ 4–4.5 min, the amplitude to be 2 nT, and its duration to be $\Delta T_0 \approx$ 32–36 min. Similar effect was observed in the magnetically conjugate region at the HON station; however, its amplitude was an order of magnitude smaller.

(5) Estimates of the bay and quasi-periodic disturbances are in good agreement with the parameters of disturbances inferred from INTERMAGNET data.

## Competing interests

The contact author has declared that none of the authors has any competing interests.

## Acknowledgments

This publication makes use of data collected during the Tonga volcanic explosion by INTERMAGFNET and published at https://www.intermagnet.org/. The solar wind parameters have been retrieved from the Goddard Space Flight Center Space Physics Data Facility https://omniweb.gsfc.nasa.gov/form/dx1.html. This research also draws upon data provided by the

World Data Center for Geomagnetism, Kyoto (data are retrieved from http://wdc.kugi.kyoto-u.ac.jp). The author was financially supported by the National Research Foundation of Ukraine (project 2020.02/0015, "Theoretical and experimental studies of global disturbances from natural and technogenic sources in the Earth-atmosphere-ionosphere system") and by Ukraine state-funded research projects #0121U109881 and #0121U109882. The author thanks Victor T. Rozumenko at V. N. Karazin Kharkiv National University for helpful comments and his help in finalizing the manuscript. Special acknowledgment is also due to Eugene G. Zhdanko for his assistance in graphic design.

**Data Availability Statement.**

The data sets discussed in this paper are freely accessible on the Internet at https://www.intermagnet.org.

**References**

Aa, E., Zhang, S.-R., Erickson, P. J., Vierinen, J., Coster, A. J., Goncharenko, L. P., Spicher, A., Rideout, W.: Significant Ionospheric Hole and Equatorial Plasma Bubbles After the 2022 Tonga Volcano Eruption. Space Weather, 20 (7), e2022SW003101, https://doi.org/10.1029/2022SW003101, 2022a.

Aa, E., Zhang, S.-R., Wang, W., Erickson, P. J., Qian, L., Eastes, R., Harding, B. J., Immel, T. J., Karan, D. K., Daniell, R. E., Coster, A. J., Goncharenko, L. P., Vierinen, J., Cai, X., and Spicher, A.: Pronounced Suppression and X-Pattern Merging of Equatorial Ionization Anomalies After the 2022 Tonga Volcano Eruption, J. Geophys. Res.: Space Physics, 127 (6), e2022JA030527. https://doi.org/10.1029/2022JA030527, 2022b.

Adushkin, V. V., Rybnov, Y. S., and Spivak, A. A.: Wave-Related, Electrical, and Magnetic Effects Due to the January 15, 2022 Catastrophic Eruption of Hunga Tonga–Hunga Ha'apai Volcano, J. Volcanolog. Seismol., 16 (4), 251–263. https://doi.org/10.1134/S0742046322040029, 2022.

Ajith, K. K., Sunil, A. S., Sunil, P. S., et al.: Atmospheric and Ionospheric Signatures Associated with the 15 January 2022 Cataclysmic Hunga-Tonga Volcanic Eruption: A Multi-layer Observation, Pure Appl. Geophys., 179, 4267–4277. https://doi.org/10.1007/s00024-022-03172-z, 2022.

Astafyeva, E., Maletckii, B., Mikesell, T. D., Munaibari, E., Ravanelli, M., Coisson, P., Manta, F., Rolland, L.: The 15 January 2022 Hunga Tonga eruption history as inferred from ionospheric observations, Geophysical Research Letters, 49 (10), e2022GL098827. https://doi.org/10.1029/2022GL098827, 2022.

Burt, S.: Multiple airwaves crossing Britain and Ireland following the eruption of Hunga Tonga–Hunga Ha'apai on 15 January 2022, Weather. Special Issue: The January 2022 eruption of Hunga Tonga-Hunga Ha'apai. 77 (3), 76–81. https://doi.org/10.1002/wea.4182, 2022.

Carvajal, M., Sepúlveda, I., Gubler, A., and Garreaud, R.: Worldwide signature of the 2022 Tonga volcanic tsunami, Geophysical Research Letters, 49 (6), e2022GL098153, https://doi.org/10.1029/2022GL098153, 2022.

Chen, C.-H., Zhang, X., Sun, Y.-Y., Wang, F., Liu, T.-C., Lin, C.-Y., Gao, Y., Lyu, J., Jin, X., Zhao, X., Cheng, X., Zhang, P., Chen, Q., Zhang, D., Mao, Z., and Liu, J.-Y.: Individual Wave Propagations in Ionosphere and Troposphere Triggered by the Hunga Tonga-Hunga Ha'apai Underwater Volcano Eruption on 15 January 2022, Remote Sensing, 14 (9), 2179, https://doi.org/10.3390/rs14092179, 2022.

Chernogor, L. F.: Advanced methods of spectral analysis of quasiperiodic wave-like processes in the ionosphere: Specific features and experimental results, Geomagn. Aeron., 48 (5), 652–673, https://doi.org/10.1134/S0016793208050101, 2008.

Chernogor, L. F.: Radiophysical and Geomagnetic Effects of Rocket Engine Burn: Monograph (in Russian), Kharkiv, V. N. Karazin Kharkiv National University Publ., 2009.

Chernogor, L. F.: Physics and ecology of the catastrophes (in Russian), Kharkiv, Ukraine, V. N. Karazin Kharkiv National University Publ., 2012.

Chernogor, L. F.: Effects of the Tonga volcano explosion on January 15, 2022, in: International Conference "Astronomy and Space Physics in the Kyiv University" in part of the World Science Day for Peace and Development. pp. 12–13, URL: http://www.observ.univ.kiev.ua/conference/wp-content/uploads/2022/10/Book_of_Abstracts-2022.pdf, 2022a.

Chernogor, L. F.: Electrical Effects of the Tonga Volcano Unique Explosion on January 15, 2022, in: International Conference "Astronomy and Space Physics in the Kyiv University" in part of the World Science Day for Peace and Development, pp. 79–80. URL: http://www.observ.univ.kiev.ua/conference/wp-content/uploads/2022/10/Book_of_Abstracts-2022.pdf, 2022b.

Chernogor, L. F., Magnetospheric Effects That Accompanied the Explosion of the Tonga Volcano on January 15, 2022, in: International Conference "Astronomy and Space Physics in the Kyiv University" in part of the World Science Day for Peace and Development, pp. 81–82. URL: http://www.observ.univ.kiev.ua/conference/wp-content/uploads/2022/10/Book_of_Abstracts-2022.pdf, 2022c.

Chernogor, L. F.: Magnetic Effects of the Unique Explosion of the Tonga Volcano, in: International Conference "Astronomy and Space Physics in the Kyiv University" in part of the World Science Day for Peace and Development, pp. 89–90. URL: http://www.observ.univ.kiev.ua/conference/wp-content/uploads/2022/10/Book_of_Abstracts-2022.pdf, 2022d.

Chernogor, L. F.: The Tonga super-volcano explosion as a subject of applied physics, in: International Scientific Conference "Electronics and Applied Physics", APHYS 2022, pp. 130–131. URL: http://www.aphys.knu.ua/index.php/history/aphys2022, 2022e.

Chernogor, L. F.: Physical effects of the January 15, 2022, powerful Tonga volcano explosion in the Earth–atmosphere–ionosphere–magnetosphere system, Space Science and Technology (in Ukrainian), 29(2 (141)), 54–77, https://doi.org/10.15407/knit2023.02.054,2023a.

Chernogor, L. F.: Ionospheric total electron content variations caused by the Tonga volcano explosion of January 15, 2022, Space Science and Technology, 29(3), 67-87, https://doi.org/10.15407/knit2023.03.067, 2023b.

Chernogor, L. F.: Global variations in the geomagnetic field caused by the explosion of the Tonga volcano on January 15, 2022, Space Science and Technology, 29(4), 2023c.

Chernogor, L. F., and Blaunstein, N.: Radiophysical and Geomagnetic Effects of Rocket Burn and Launch in the Near-the-Earth Environment, Boca Raton, London, New York: CRC Press. Taylor & Francis Group, https://doi.org/10.1201/b15614, 2013.

Chernogor, L. F., and Holub, M. Yu.: Large-scale geomagnetic field disturbances accompanied by the powerful explosion of the Tonga volcano on January 15, 2022, Visnyk of V. N. Karazin Kharkiv National University, Radio Physics and Electronics Series, in press, 2023a.

Chernogor, L. F., and Holub, M. Yu.: Bay-shaped variations in the geomagnetic field that accompanied the catastrophic explosion of the Tonga volcano on January 15, 2022, Kinematics and Physics of Celestial Bodies, in press, 2023b.

Chernogor, L. F., and Shevelev, M. B.: A statistical study of the explosive waves launched by the Tonga super-volcano on January 15, 2022, Space Science and Technology, in press, 2023.

Chernogor, L. F, and Shevelev, M. B.: Statistical characteristics of atmospheric waves, generated by the explosion of the Tonga volcano on January 15, 2022, in: International Conference "Astronomy and Space Physics in the Kyiv University" in part of the World Science Day for Peace and Development, pp. 85–86. URL: http://www.observ.univ.kiev.ua/conference/wp-content/uploads/2022/10/Book_of_Abstracts-2022.pdf, 2022.

Diaz, J.: Atmosphere-solid earth coupling signals generated by the 15 January 2022 Hunga-Tonga eruption, Commun Earth Environ, 3, 281, https://doi.org/10.1038/s43247-022-00616-1, 2022.

Harding, B. J., Wu, Y.-J.J., Alken, P., Yamazaki, Y., Triplett, C. C., Immel, T. J., Gasque, L. C., Mende, S. B., and Xiong, C.: Impacts of the January 2022 Tonga Volcanic Eruption on the Ionospheric Dynamo: ICON-MIGHTI and Swarm Observations of Extreme Neutral Winds and Currents, Geophysical Research Letters, 49 (9), e2022GL098577. https://doi.org/10.1029/2022GL098577, 2022.

Hong, J., Kil, H., Lee, W. K., Kwak, Y.-S., Choi, B.-K., Paxton, and L. J.: Detection of different properties of ionospheric perturbations in the vicinity of the Korean Peninsula after the Hunga-Tonga volcanic eruption on 15 January 2022, Geophysical Research Letters, 49, e2022GL099163, https://doi.org/10.1029/2022GL099163, 2022.

Imamura, F., Suppasri, A., Arikawa, T., Koshimura, S., Satake, K., and Tanioka, Y.: Preliminary Observations and Impact in Japan of the Tsunami Caused by the Tonga Volcanic Eruption on January 15, 2022, Pure and Applied Geophysics, 179, 1549–1560, https://doi.org/10.1007/s00024-022-03058-0, 2022.

Iyemori, T., Nishioka, M., Otsuka, Y., et al.: A confirmation of vertical acoustic resonance and field-aligned current generation just after the 2022 Hunga Tonga Hunga Ha'apai volcanic eruption, Earth Planets Space, 74, 103, https://doi.org/10.1186/s40623-022-01653-y, 2022.

Kubota, T., Saito, T., and Nishida, K.: Global fast-traveling tsunamis driven by atmospheric Lamb waves on the 2022 Tonga eruption, Science, 377 (6601), 91–94, https://doi.org/10.1126/science.abo4364, 2022.

Kulichkov, S. N., Chunchuzov, I. P., Popov, O. E., Gorchakov, G. I., Mishenin, A. A., Perepelkin, V. G., Bush, G. A., Skorokhod, A. I., Vinogradov, Yu. A., Semutnikova, E. G., Šepic, J., Medvedev, I. P., Gushchin, R. A., Kopeikin, V. M., Belikov, I. B., Gubanova, D. P., Karpov, A. V., and Tikhonov, A. V.: Acoustic-Gravity Lamb Waves from the Eruption of the Hunga-Tonga-Hunga-Hapai Volcano, Its Energy Release and Impact on Aerosol Concentrations and Tsunami, Pure and Applied Geophysics, 179, 1533–1548, https://doi.org/10.1007/s00024-022-03046-4, 2022.

Le, G., Liu, G., Yizengaw, E., and Englert, C. R.: Intense equatorial electrojet and counter electrojet caused by the 15 January 2022 Tonga volcanic eruption: Space- and ground-based observations, Geophysical Research Letters, 49 (11), e2022GL099002, https://doi.org/10.1029/2022GL099002, 2022.

Lin, J.-T., Rajesh, P. K., Lin, C. C. H., Chou, M.-Y., Liu, J.-Y., Yue, J., Hsiao, T.-Y., Tsai, H.-F., Chao, H.-M., and Kung, M.-M.: Rapid Conjugate Appearance of the Giant Ionospheric Lamb Wave Signatures in the Northern Hemisphere After Hunga-Tonga Volcano Eruptions, Geophysical Research Letters, 49 (8), e2022GL098222, https://doi.org/10.1029/2022GL098222, 2022.

Matoza, R. S., Fee, D., Assink, J. D., Iezzi, A. M., Green, D. N., Kim, K., Toney, L., Lecocq, T., Krishnamoorthy, S., Lalande, J. M., Nishida, K., Gee, K. L., Haney, M. M., Ortiz, H. D., Brissaud, Q., Martire, L., Rolland, L., Vergados, P., Nippress, A., Park, J., Shani-Kadmiel, S., Witsil, A., Arrowsmith, S., Caudron, C., Watada, S., Perttu, A. B., Taisne, B., Mialle, P., Le Pichon, A., Vergoz, J., Hupe, P., Blom, P. S., Waxler, R., De Angelis, S., Snively, J. B., Ringler, A. T., Anthony R. E., Jolly A. D., Kilgour G., Averbuch G., Ripepe M., Ichihara M., Arciniega-Ceballos, A., Astafyeva, E., Ceranna, L., Cevuard, S., Che, I.-Y., De Negri, R., Ebeling, C. W., Evers, L. G., Franco-Marin, L. E., Gabrielson, T. B., Hafner, K., Harrison, R. G., Komjathy, A., Lacanna, G., Lyons, J., Macpherson, K. A., Marchetti, E., McKee, K. F., Mellors, R. J., Mendo-Pérez, G., Mikesell, T. D., Munaibari, E., Oyola-Merced, M., Park, I., Pilger, C., Ramos, C., Ruiz, M. C., Sabatini, R., Schwaiger, H. F., Tailpied, D., Talmadge, C., Vidot, J., Webster, J., and Wilson, D. C.: Atmospheric waves and global seismoacoustic observations of the January 2022 Hunga eruption, Tonga, Science, 377 (6601), 95–100, https://doi.org/10.1126/science.abo7063, 2022a.

Matoza, R. S., Fee, D., Assink, J. D., Iezzi, A. M., Green, D. N., Kim, K., Toney, L., Lecocq, T., Krishnamoorthy, S., Lalande, J. M., Nishida, K., Gee, K. L., Haney, M. M., Ortiz, H. D., Brissaud, Q., Martire, L., Rolland, L., Vergados, P., Nippress, A., Park, J., Shani-Kadmiel, S., Witsil, A., Arrowsmith, S., Caudron, C., Watada, S., Perttu, A. B., Taisne, B., Mialle, P., Le Pichon, A., Vergoz, J., Hupe, P., Blom, P. S., Waxler, R., De Angelis, S., Snively, J. B., Ringler, A. T., Anthony R. E., Jolly A. D., Kilgour G., Averbuch G., Ripepe M., Ichihara M., Arciniega-Ceballos, A., Astafyeva, E., Ceranna, L., Cevuard, S., Che, I.-Y., De Negri, R., Ebeling, C. W., Evers, L. G., Franco-Marin, L. E., Gabrielson, T. B., Hafner, K., Harrison, R. G., Komjathy, A., Lacanna, G., Lyons, J., Macpherson, K. A., Marchetti, E., McKee, K. F., Mellors, R. J., Mendo-Pérez, G., Mikesell, T. D., Munaibari, E., Oyola-Merced, M., Park, I., Pilger, C., Ramos, C., Ruiz, M. C., Sabatini, R., Schwaiger, H. F., Tailpied, D., Talmadge, C., Vidot, J., Webster, J., and Wilson, D. C.: Supplementary Materials for Atmospheric waves and global seismoacoustic observations of the January 2022 Hunga eruption, Tonga, Science, 377 (6601), https://doi.org/10.1126/science.abo7063, 2022b.

McNutt, S. R., Thompson, G., Johnson, J., De Angelis, S., and Fee, D.: The Encyclopedia of Volcanoes (Second Edition), Academic Press, https://doi.org/10.1016/B978-0-12-385938-9.00063-8, 2015.

Muafiry, I. N., Meilano, I., Heki, K., Wijaya, and D. D., Nugraha, K. A.: Ionospheric Disturbances after the 2022 Hunga Tonga-Hunga Ha'apai Eruption above Indonesia from GNSS-TEC Observations, Atmosphere, 13, 1615, https://doi.org/10.3390/atmos13101615, 2022.

Otsuka, S.: Visualizing Lamb waves from a volcanic eruption using meteorological satellite Himawari-8, Geophysical Research Letters, 49 (8), e2022GL098324, https://doi.org/10.1029/2022GL098324, 2022.

Poli, P., and Shapiro, N. M.: Rapid Characterization of Large Volcanic Eruptions: Measuring the Impulse of the Hunga Tonga Ha'apai Explosion From Teleseismic Waves, Geophysical Research Letters, 49 (8), e2022GL098123, https://doi.org/10.1029/2022GL098123, 2022.

Rakesh, V., Haridas, S., Sivan, C., Manoj, M. G., Abhilash, S., Paul, B., Unnikrishnan, K., Mohanakumar, K., and Chandran, R. S.: Impact of the Hunga Tonga-Hunga Ha'apai volcanic eruption on the changes observed over the Indian near-equatorial ionosphere, Advances in Space Research, 70 (8), 2480–2493, https://doi.org/10.1016/j.asr.2022.07.004, 2022.

Ramírez-Herrera, M. T., Coca, O., and Vargas-Espinosa, V.: T`ami Effects on the Coast of Mexico by the Hunga Tonga-Hunga Ha'apai Volcano Eruption, Tonga, Pure and Applied Geophysics, 179, 1117–1137, https://doi.org/10.1007/s00024-022-03017-9, 2022.

Schnepf, N. R., Minami, T., Toh, H., and Nair, M. C.: Magnetic Signatures of the 15 January 2022 Hunga Tonga–Hunga Ha'apai Volcanic Eruption, Geophysical Research Letters, 49 (10), e2022GL098454, https://doi.org/10.1029/2022GL098454, 2022.

Shinbori, A., Otsuka, Y., Sori, T., et al.: Electromagnetic conjugacy of ionospheric disturbances after the 2022 Hunga Tonga-Hunga Ha'apai volcanic eruption as seen in GNSS-TEC and SuperDARN Hokkaido pair of radars observations, Earth Planets Space, 74, 106, https://doi.org/10.1186/s40623-022-01665-8, 2022.

Soares, G., Yamazaki, Y., and Matzka, J.: Localized geomagnetic disturbance due to ionospheric response to the Hunga Tonga eruption on January 15, 2022, Geophysical Research Letters, https://doi.org/10.1002/essoar.10510482.1, 2022.

Sorokin, V. M., and Fedorovich, G. V.: The physics of slow MHD waves in the ionospheric plasma (in Russian), Moscow, Energoatomizdat, https://ui.adsabs.harvard.edu/abs/1982MEner....T....S/abstract, 1982.

Sun, Y.-Y.; Chen, C.-H.; and Lin, C.-Y.: Detection of Vertical Changes in the Ionospheric Electron Density Structures by the Radio Occultation Technique Onboard the FORMOSAT-7/COSMIC2 Mission over the Eruption of the Tonga Underwater Volcano on 15 January 2022, Remote Sens., 14, 4266. https://doi.org/10.3390/rs14174266, 2022a.

Sun, Y.-Y., Chen, C.-H., Zhang, P., Li, S., Xu, H.-R., Yu, T., et al.: Explosive eruption of the Tonga underwater volcano modulates the ionospheric E-region current on 15 January 2022, Geophysical Research Letters, 49, e2022GL099621, https://doi.org/10.1029/2022GL099621, 2022b.

Tanioka, Y., Yamanaka, Y., and Nakagaki, T.: Characteristics of the deep sea tsunami excited offshore Japan due to the air wave from the 2022 Tonga eruption, Earth, Planets and Space, 74, 61. https://doi.org/10.1186/s40623-022-01614-5, 2022.

Terry, J. P., Goff, J., Winspear, N., Bongolan, V. P., and Fisher, S.: Tonga volcanic eruption and tsunami, January 2022: globally the most significant opportunity to observe an explosive and tsunamigenic submarine eruption since AD 1883 Krakatau, Geoscience Letters, 9, 24, https://doi.org/10.1186/s40562-022-00232-z, 2022.

Themens, D. R., Watson, C., Žagar, N., Vasylkevych, S., Elvidge, S., McCaffrey, A., Prikryl, P., Reid, B., Wood, A., and Jayachandran, P. T.: Global propagation of ionospheric disturbances associated with the 2022 Tonga volcanic eruption, Geophysical Research Letters, 49 (7), e2022GL098158, https://doi.org/10.1029/2022GL098158, 2022.

Wright, C. J., Hindley, N. P., Alexander, M. J., et al.: Surface-to-space atmospheric waves from Hunga Tonga–Hunga Ha'apai eruption, Nature, 609, 741–746, https://doi.org/10.1038/s41586-022-05012-5, 2022.

Yamazaki, Y., Soares, G., and Matzka, J.: Geomagnetic Detection of the Atmospheric Acoustic Resonance at 3.8 mHz During the Hunga Tonga Eruption Event on 15 January 2022, Journal of Geophysical Research: Space Physics, 127 (7), e2022JA030540, https://doi.org/10.1029/2022JA030540, 2022.

Yuen, D. A., Scruggs, M. A., Spera, F. J., Zheng, Y., Hu, H., McNutt, S. R., Thompson, G., Mandli, K., Keller, B. R., Wei, S. S., Peng, Z., Zhou, Z., Mulargia, F., and Tanioka, Y.: Under the surface: Pressure-induced planetary-scale waves, volcanic lightning, and gaseous clouds caused by the submarine eruption of Hunga Tonga-Hunga Ha'apai volcano, Earthquake Research Advances, 2 (3), 100134, https://doi.org/10.1016/j.eqrea.2022.100134, 2022.

Zhang, S.-R., Vierinen, J., Aa, E., Goncharenko, L. P., Erickson, P. J., Rideout, W., Coster, A. J., and Spicher, A., 2022 Tonga Volcanic Eruption Induced Global Propagation of Ionospheric Disturbances via Lamb Waves, Frontiers in Astronomy and Space Sciences, 9, 871275: https://doi.org/10.3389/fspas.2022.871275, 2022a.

Zhang, J., Xu, J., Wang, W., Wang, G., Ruohoniemi, J. M., Shinbori, A., et al.: Oscillations of the ionosphere caused by the 2022 Tonga volcanic eruption observed with SuperDARN radars, Geophysical Research Letters, 49, e2022GL100555, https://doi.org/10.1029/2022GL100555, 2022b.